

UCLA

UCLA Previously Published Works

Title

Emulsion-templated microparticles with tunable stiffness and topology: Applications as edible microcarriers for cultured meat

Permalink

<https://escholarship.org/uc/item/4kx288f1>

Authors

Norris, Sam CP  
Kawecki, N Stephanie  
Davis, Ashton R  
et al.

Publication Date

2022-08-01

DOI

10.1016/j.biomaterials.2022.121669

Peer reviewed



Published in final edited form as:

*Biomaterials*. 2022 August ; 287: 121669. doi:10.1016/j.biomaterials.2022.121669.

## Emulsion-templated microparticles with tunable stiffness and topology: Applications as edible microcarriers for cultured meat

Sam C.P. Norris<sup>a</sup>, N. Stephanie Kawecki<sup>a,b</sup>, Ashton R. Davis<sup>a,c</sup>, Kathleen K. Chen<sup>a,c</sup>, Amy C. Rowat<sup>a,b,d,e,f,\*</sup>

<sup>a</sup> Department of Integrative Biology and Physiology, University of California, Los Angeles, Los Angeles, CA 90095, USA

<sup>b</sup> Department of Bioengineering, University of California, Los Angeles, Los Angeles, CA 90095, USA

<sup>c</sup> Department of Chemistry and Biochemistry, University of California, Los Angeles, Los Angeles, CA 90095, USA

<sup>d</sup> Jonsson Comprehensive Cancer Center, University of California, Los Angeles, Los Angeles, CA 90095, USA

<sup>e</sup> Broad Stem Cell Center, University of California, Los Angeles, Los Angeles, CA 90095, USA

<sup>f</sup> California NanoSystems Institute, University of California, Los Angeles, Los Angeles, CA 90095, USA

### Abstract

Cultured meat has potential to diversify methods for protein production, but innovations in production efficiency will be required to make cultured meat a feasible protein alternative. Microcarriers provide a strategy to culture sufficient volumes of adherent cells in a bioreactor that are required for meat products. However, cell culture on inedible microcarriers involves extra downstream processing to dissociate cells prior to consumption. Here, we present edible microcarriers that can support the expansion and differentiation of myogenic cells in a single bioreactor system. To fabricate edible microcarriers with a scalable process, we used water-in-oil emulsions as templates for gelatin microparticles. We also developed a novel embossing technique to imprint edible microcarriers with grooved topology in order to test if microcarriers with

This is an open access article under the CC BY-NC-ND license (<http://creativecommons.org/licenses/by-nc-nd/4.0/>).

\* Corresponding author. Department of Integrative Biology and Physiology, University of California, Los Angeles, Los Angeles, CA 90095, USA. rowat@ucla.edu (A.C. Rowat).

#### Author statement

Sam C.P. Norris: Conceptualization, Methodology, Validation, Formal Analysis, Investigation, Data Curation, Writing – Original Draft, Writing – Review & Editing, Visualization. N. Stephanie Kawecki: Conceptualization, Methodology, Validation, Formal Analysis, Investigation, Writing – Review & Editing, Visualization, Funding Acquisition. Ashton R. Davis: Methodology, Formal Analysis, Investigation, Writing – Review & Editing, Visualization, Funding Acquisition. Kathleen K. Chen: Conceptualization, Methodology, Writing – Review & Editing. Amy C. Rowat: Conceptualization, Methodology, Resources, Writing – Original Draft, Writing – Review & Editing, Visualization, Supervision, Project Administration, Funding Acquisition.

#### Declaration of competing interest

The authors declare that they have no known competing financial interests or personal relationships that could have appeared to influence the work reported in this paper.

#### Appendix A. Supplementary data

Supplementary data to this article can be found online at <https://doi.org/10.1016/j.biomaterials.2022.121669>.

striated surface texture can promote myoblast proliferation and differentiation in suspension culture. In this proof-of-concept demonstration, we showed that edible microcarriers with both smooth and grooved surface topologies supported the proliferation and differentiation of mouse myogenic C2C12 cells in a suspension culture. The grooved edible microcarriers showed a modest increase in the proliferation and alignment of myogenic cells compared to cells cultured on smooth, spherical microcarriers. During the expansion phase, we also observed the formation of cell-microcarrier aggregates or ‘microtissues’ for cells cultured on both smooth and grooved microcarriers. Myogenic microtissues cultured with smooth and grooved microcarriers showed similar characteristics in terms of myotube length, myotube volume fraction, and expression of myogenic markers. To establish feasibility of edible microcarriers for cultured meat, we showed that edible microcarriers supported the production of myogenic microtissue from C2C12 or bovine satellite muscle cells, which we harvested by centrifugation into a cookable meat patty that maintained its shape and exhibited browning during cooking. These findings demonstrate the potential of edible microcarriers for the scalable production of cultured meat in a single bioreactor.

## Keywords

Cellular agriculture; Mechanobiology; Tissue engineered skeletal muscle; Hydrogel; Scaffold

---

## 1. Introduction

Diversifying methods for protein production will be critical for the future of food systems. Livestock provide a major source of dietary protein, but with the world’s growing population and susceptibility to climate variability [1], innovative protein production systems will be critical to meet human consumption and nutritional needs into the future. Reducing industrial-scale meat production could decrease greenhouse gas emissions and animal waste runoff, and thereby improve environment and human health [2–5]. Alternative methods for meat production could also protect against supply chain disruptions during epidemics and natural disasters [6]. Plant-based meats provide protein alternatives that have experienced rapid growth and market demand but the majority of consumers still want to eat real meat [7,8]. The rapidly developing field of cultured meat—which addresses the challenge of growing muscle *ex vivo* by culturing precursor cells harvested from animals in a bioreactor—could provide a complementary method for meat production. Life cycle assessments (LCA) have shown that cultured meat production has potential to achieve significant reductions in greenhouse gas emissions and land use compared to industrial meat production [9–11]. However, it will be critical to produce cultured meat with desired sensory and nutrient qualities that consumers crave [12].

The generation of skeletal muscle tissue *in vitro* at the laboratory scale has been enabled by tissue engineering and biomaterial approaches for decades [13–15], such as 3D printed scaffolds [16,17] or nanofiber sheets [18]; these developments have provided a foundation for the rapid emergence of cultured meat technologies. To produce cultured meat as a food source, however, requires  $\sim 10^{11}$  cells for a single kg of animal meat [19]. One approach is to adapt cells to grow in suspension in a bioreactor, but *in vivo*, cells in muscle tissue (including precursor myoblasts, satellite muscle cells, and myotubes) are attached to the

extracellular matrix (ECM). The ECM plays an important role in the development of skeletal muscle [20,21]. For example, the ECM localizes growth factors that influence the proliferation and differentiation of muscle satellite cells [22]. Substrate surface topology has been shown through in vitro experiments to impact C2C12 cell proliferation and differentiation [23]. Substrate stiffness regulates both the differentiation of myoblasts [24] and skeletal muscle stem cell expansion [25]. Initial demonstrations of suspension culture of bovine myoblasts in a spinner flask bioreactor used inert microcarriers such as dextran (Cytodex) beads [26], which have been established as a growth surface to support the proliferation and differentiation of various types of animal cells [27, 28]. However, the required dissociation of cells from inedible microcarriers for cultured meat applications adds complexity to downstream processing [19,29]. To increase process efficiency—which is especially important for large scale cultures [26]—edible scaffolds provide a promising approach [30–32]. Scaffolds made of natural materials with inherent porous structure, such as textured soy protein, can support the growth and differentiation of myoblasts [33]. Scaffolds can also be engineered from edible materials to have a fibrous structure that mimics the native striated architecture of skeletal muscle [34]. Importantly, proof-of-concept demonstrations establish that centimeter-scale pieces of cultured meat can be generated using edible scaffolds and cooked to achieve desired sensory properties [33,34]. Specific spatial patterns in engineered tissues comprised of cells and edible scaffolds can also be achieved using 3D printing [35]. For maximum scale-up potential, however, scaffolds need to be compatible with bioreactors. One way to improve efficiency of cultured meat in a bioreactor would be to culture myoblasts on edible microcarriers with tunable physical properties to effectively drive their proliferation and differentiation into myotubes.

In this study, we aimed to develop edible microcarriers with tunable mechanics and surface topology for cultured meat applications. To establish proof-of-concept for this approach, we fabricated microcarriers using gelatin and the food-grade crosslinking enzyme, microbial transglutaminase (MTG). Importantly, our process does not require the use of any synthetic polymers, additional small molecule chemical crosslinking agents, or chemical modification of the protein side groups. We developed a scalable process to generate edible microcarriers using water-in-oil emulsions, which enabled us to readily fabricate hydrogel microparticles with a spherical shape and smooth surface. Based on previous findings that striated substrates promote myoblast proliferation [23] and myotube formation [23,36], we also developed an embossing method to imprint grooved surface topology on edible microcarriers to determine if microcarrier surface topology enhances myogenesis. The main goal of the study was to test the utility of the smooth and spherical as well as grooved edible microcarriers to support the culture of myogenic tissue for cooking applications.

## 2. Materials and methods

### 2.1. Fabrication of edible spherical gelatin microcarriers

To fabricate edible spherical microcarriers (sMCs), we adapted previously established techniques for creating gelatin particles using water-in-oil emulsions [37–39]. To produce microcarriers with varying stiffness, we generated prepolymer solutions of gelatin derived from bovine skin (Sigma, Type B) and microbial transglutaminase (MTG) powder (Activia



We then placed the entire sandwich in a humidified 37 °C incubator to finish crosslinking (see Table 1 for crosslinking times). The PDMS stamps were then peeled apart and the microcarriers were released from the stamps by washing with a pressurized stream of water and collected with a 100 µm filter (PluriSelect). Excess oil was washed away during filtration. The collected gMCs were suspended in 1 × PBS with 0.1% Tween 80, and placed in an 80 °C water bath for 10 min to inactivate any remaining transglutaminase. The gMCs were then washed three times with 1 × PBS with 0.1% Tween 80 and incubated overnight to ensure complete swelling before use.

### 2.3. Characterization of microcarriers by atomic force microscopy (AFM)

The Young's modulus and topology of the gelatin microcarriers were measured in 1 × PBS with 0.1% Tween 80 using a JPK Nanowizard 4a BioScience AFM in force spectroscopy mode. The microcarriers were adhered to a poly-lysine coated slide (Epredia) and indented with a SAA-SPH-5UM probe (Bruker) with a 10 µm diameter spherical tip. The spring constants of the probes were individually calibrated by the manufacturer. Single indentations were performed with a total force of 4.0 nN. Since an oblique contact between the spherical AFM probe and the microcarrier surface can result in inaccurate force curve fitting, indentations were performed on the top surface of the microcarriers (the top of the ridges of the gMCs or the apex of the sMCs). Young's modulus values were determined by averaging over 5 unique indentations for sMCs and over at least 15 unique indentations along the top of multiple parallel ridges for gMCs. All force curve analysis was performed using the JPK Data Processing software. The Young's modulus was calculated by using a Hertz/Sneddon spherical fit with a Poisson's ratio of  $\nu = 0.5$  [43].

### 2.4. Preparation of microcarriers for cell culture

Prior to cell culture, microcarriers were sterilized in 70% ethanol for 10 min, then washed three times with sterile 1 × PBS with 0.1% Tween 80. Cytodex 1 microcarriers (Sigma) were prepared according the manufacturer's instructions. To maintain a consistent ratio of cells to microcarrier surface area, we first determined the microcarrier surface area per culture volume by quantitative image analysis. Fluorescent images of a suspension of a defined 10 µL volume of microcarriers tagged with fluorescein-5-Isothiocyanate (FITC, ThermoFisher) were acquired using multi-tile image acquisition. Images of microcarriers were segmented using a deep learning segmentation algorithm (Cellpose [44]). To determine the size of the spherical sMC and Cytodex microcarriers, as well as the flattened gMC disc microcarriers, we analyzed the segmented images using a custom algorithm (MATLAB); the measured radii were used to calculate the surface area ( $A$ ) of the microcarriers for spherical ( $A = 4\pi r^2$ ) and disc geometries ( $A = 2 \times \pi r^2$ , where the extra factor of two accounts for both sides of the discs). With our goal to determine the available microcarrier surface area for cell attachment, we considered only the projected surface area of both sides of the gMC disc. We did not include the extra surface area from the edges of the gMCs or the vertical sidewalls of the grooves, as we assumed these do not contribute substantially to the effective cell-detectable surface area; this assumption is consistent with observations that the strongest attachment of cells occurs on the horizontal regions of grooves [45]. We then determined the total microcarrier surface area per culture volume in units of  $\text{cm}^2/\text{mL}$  by measuring the total number and surface area of all microcarriers in a 10 µL aliquot. For the

sMCs and gMCs, stock suspensions typically had a surface area concentration of ~10–50 cm<sup>2</sup>/mL. For the Cytodex 1 microcarriers, we prepared a stock solution with 10 mg dry Cytodex per mL stock suspension, which corresponds to a surface area concentration of 42 cm<sup>2</sup>/mL. For all experiments, we used a seeding density of ~11,400 cells/cm<sup>2</sup> (8.8 cm<sup>2</sup>/mL of microcarriers and 100,000 cells/mL), which is recommended by the manufacturer of the Cytodex microcarriers [27] and similar to seeding densities used in previous studies to generate 3D tissue constructs [46,47].

## 2.5. Cell culture

Mouse myoblasts (C2C12, ATCC CRL-1772) were cultured in Dulbecco's Modified Eagle's Medium (DMEM) (Gibco, 4.5 g/L glucose, L-glutamine, 110 mg/L sodium pyruvate) with 10% fetal bovine serum (FBS, GemCell™, Gemini) and 1 × antibiotic-antimycotic (Gibco). We confirmed cell line identity by STR profiling. To induce differentiation of C2C12 cells into myotubes, we cultured cells in differentiation induction medium consisting of DMEM with 2% donor horse serum (HS, Gemini GemCell™) and 1 × antibiotic-antimycotic (Gibco). C2C12 cells were cultured for 10 passages at 37 °C and 5% CO<sub>2</sub>. Bovine satellite muscle cells (BSMCs, a gift from the lab of David Kaplan, Tufts University) were cultured in DMEM high glucose, GlutaMAX™ (Gibco, 4.5 g/L glucose, L-alanine-L-glutamine, 110 mg/L sodium pyruvate) with 20% FBS, 1 ng/mL recombinant bovine basic fibroblast growth factor (bFGF2, Novus Biologicals) and 1 × antibiotic-antimycotic. To induce differentiation of BSMCs into myotubes, cells were cultured in proliferation media for one week without media changes. BSMCs were cultured for <6 passages at 37 °C and 5% CO<sub>2</sub>.

For suspension culture of C2C12 cells and microcarriers during expansion and differentiation experiments, cultures were placed in siliconized scintillation vials (20 mL, DWK Life Science) on a nutating mixer (Clay Adams, 24 RPM). Motivated by previous findings on the optimal matrix stiffness for C2C12 differentiation into myotubes [24], we used gelatin microcarriers with ~14 kPa stiffness: 9 wt% and 24 h crosslinking for the sMCs; and 9 wt% and 8 h crosslinking for the gMCs (see Table 1 for composition details). To promote cell adhesion to the microcarriers, cells were inoculated into ~1/3 of the final culture volume and intermittently stirred for 1 min every 45 min for 3 h, after which the culture was diluted to the final volume and stirred continuously [27]. Approximately 50% of the volume of cell culture media was replaced daily with fresh media. For larger-scale cultured bovine meat experiments, we cultured bovine skeletal muscle cells in a 25 mL or 100 mL stirrer flask (Bellco Glass) agitated using a magnetic stirrer at 60 RPM; these stirrer flasks have features similar to larger scale bioreactors and are commonly used for laboratory scale studies [48].

## 2.6. Cell proliferation assay

To quantify the growth of cells on microcarriers, we used a Qubit dsDNA BR assay (Invitrogen) to measure genomic DNA as a function of culture time. We found that the microtissues did not consistently dissociate into individual cells by application of trypsin, and edible microcarriers and microtissue aggregates tended to clog the orifice of nucleocounter devices. Therefore we used a method to lyse the entire cell-microcarrier aggregates and measure genomic DNA as described previously to quantify the growth

of muscle satellite cells on microcarriers [26]. DNA was quantified according to the manufacturer's instructions with slight optimization. We initiated cultures by placing  $3.3 \times 10^5$  cells in scintillation vials with a total of 3.3 mL cell culture media and microcarriers with total 29.0 cm<sup>2</sup> surface area to give 11,400 cells/cm<sup>2</sup> for all three types of microcarriers. To quantify cells over the 8-day proliferation period, we removed 300  $\mu$ L aliquots from the cell-microcarrier suspensions at days 0, 2, 4, 6, and 8. At each time point, the cell-microcarrier suspension was pelleted, lysed (RTL buffer, Qiagen), and heated in a 55 °C water bath for 10 min with intermittent vortexing. The mixture was centrifuged at 10,000 RCF for 5 min and the supernatant was mixed with the Qubit working solution. The fluorescence intensity of the mixtures was measured with excitation = 485 nm and emission = 530 nm with a Spectramax M2 plate reader (Molecular Devices). The amount of DNA was quantified against a standard curve and the number of cells was quantified assuming 6.6 pg of DNA per cell [49]. While each aliquot that we removed for cell quantification should theoretically contain an equivalent amount of surface area across all three microcarrier types, we observed that cells grew into the interstitial spaces between microcarriers within the aggregates, and were not always attached to a microcarrier surface; therefore we report the cell concentration in cells per mL of culture volume.

## 2.7. Imaging cell-microcarrier microtissues

To visualize cells and myotubes in microtissues, we adapted a protocol that was developed to fix tissue samples with ~1 mm thickness [50]. In brief, cell-microcarrier constructs or "microtissues" were fixed with 4% paraformaldehyde (Fisher) in 1  $\times$  PBS for 24 h at 4 °C. Samples were then permeabilized and treated with a blocking solution of 0.1% Triton X-100 (Amresco) and 1% bovine serum albumin (BSA) (Fisher) in PBS for 24 h before labeling for myosin heavy chain (MF20, eBioscience™, Invitrogen and Alexa-Fluor 594 goat anti-mouse, Invitrogen), F-actin (Alexa 633-conjugated phalloidin, Invitrogen), and DNA (Hoechst 33342, trihydrochloride trihydrate, Life Technologies) for an additional 24 h. Labeled samples were mounted using Fluoromount-G (Invitrogen) and imaged using a laser scanning confocal microscope (Zeiss LSM880) equipped with a 10  $\times$  /0.45 NA or 20  $\times$  /0.8 NA objective, and using a pinhole of 1 AU. All widefield images were acquired with a Zeiss Observer Z1 using a 5  $\times$  /0.13 NA, 10  $\times$  /0.31 NA, or 20  $\times$  /0.5 NA objective.

Images were processed with Zen (Zeiss), Fiji, and Imaris (Bitplane) software. To characterize cell morphology during the expansion phase, cells and nuclei were segmented using Cellpose. Using a custom MATLAB program, individual cell bodies and nuclei were fit to an ellipse that has the same normalized second central moments as the segmented region. Using the same algorithm, the cell spread area was determined. We used the major and minor axis of the fitted ellipse to determine the cellular length and width, respectively. For cells on the gMCs, we quantified alignment of the cell major axis with the groove direction by determining the orientation angle ( $\theta$ ) of cells and nuclei, which is the angle between the major axis of the fitted ellipse and the gMC groove direction. The orientation angle ( $\theta$ ) of cells on sMCs and Cytodex microcarriers was measured as the relative angle between the major axis of the fitted ellipse and the average major cell axis direction.



To determine the volume fraction of myotubes and cellular matter, individual voxels were classified as either gelatin, nucleus, myotubes, F-actin, or empty space using a machine learning software (Ilastik [51]). The fraction of cellular material was determined as the number of voxels occupied by cell material (nucleus, myotube, F-actin) divided by the total number of voxels in the microtissue (including microcarriers). Voxels were classified based on their fluorescence color and intensity as well as the shape and size of the objects being classified. To determine the volume fraction of myotubes, the number of differentiated muscle cell voxels was divided by the total number of voxels in the microtissue belonging to cell material. To quantify the length of the myotubes, we manually traced the path of the myotubes in the 3D confocal images for all three microcarrier types. To quantify the total number of nuclei per volume of tissue, Cellpose [44] was used to delineate nuclei in 3D stacks of confocal images. The total number of nuclei identified was divided by the total volume of tissue analyzed; cells on the edge of the imaging volume were excluded.

To quantify the degree of F-actin alignment across length scales from 1 to 100  $\mu\text{m}$ , we applied a Fourier transform (FT) image analysis technique to extract an ‘orientation index’ (OI) [52]. Details on the calculation of the orientation index and code for the calculations have been described previously [53]. Briefly, a custom MATLAB program was written that randomly selected square regions of dimensions 1.60–128  $\mu\text{m}$  in length within the F-actin stained images, with the requirement that all pixels comprised cellular matter. The absolute value of the shifted FT was converted into polar coordinates ( $r, \phi$ ) to produce the FT power spectrum. Here, the strength of the different angle bands within the FT is an indicator of fiber alignment. The magnitude of the FT was calculated as a function of  $\phi$  by integrating across  $r$  to give the FT power spectrum line average  $I_{FT}(\phi)$ , which was shifted such that the maximum of  $I_{FT}(\phi)$  was located at  $\phi = 0$ . The OI was calculated using the equation [54]:

$$\text{OI} = [2(\cos^2\phi) - 1] \times 100\%,$$

where

$$\cos^2\phi = \frac{\int_{-\pi/2}^{\pi/2} I_{FT}(\phi) \cos^2\phi d\phi}{\int_{-\pi/2}^{\pi/2} I_{FT}(\phi) d\phi}.$$

The orientation index spans from 0 to 100, where an index of 0 indicates an isotropic distribution of actin with no directionality and an index of 100 indicates perfectly aligned actin fibers across the length scale of interest.

## 2.8. Real-time quantitative polymerase chain reaction (RT-qPCR)

To measure the extent of C2C12 myogenic differentiation on microcarriers, we performed RT-qPCR. We conducted whole-cell RNA extraction using TRIzol® reagent (Invitrogen) according to the manufacturer’s protocol. Total RNA was further purified using the PureLink™ RNA Mini Kit (Invitrogen). Reverse transcriptase was performed to obtain cDNA using the SuperScript™ IV First-Strand Synthesis System (Invitrogen). RT-qPCR was performed using the QuantStudio™ 5 Real-Time PCR System (Applied Biosystems)

and PowerUp™ SYBR™ Green Master Mix (Applied Biosystems) with the gene-specific primers as given in Table 2. Cells in the undifferentiated control group were cultured for 24 h in growth media prior to RNA extraction. Cells in the differentiated group were cultured for 7 days in growth media, after which the media was exchanged for differentiation media and cells were cultured for an additional 7 days before extraction. Changes in gene expression were quantified using the delta delta cycle time method ( $\Delta\Delta C_t$ ) with *Gapdh* as an endogenous control. Transcript levels were normalized to a control of undifferentiated C2C12 cells on tissue culture plastic (TCP) after 1 day in culture.

## 2.9. Harvesting and cooking cultured meat

We harvested microtissues from stirred-flasks bioreactors by centrifuging the suspension at 1000 RCF for 10 min. To promote fusion of microtissues into a cohesive piece of cultured meat, excess culture media was removed and the microtissues were mixed with a solution of 3 w/w % gelatin and 4 w/w% MTG powder and allowed to incubate for 12 h at 37 °C. To cook the cultured meat, we placed the meat in a Teflon pan that was placed on top of a hotplate with a surface temperature of 195 °C. The cultured meat was cooked in olive oil until brown. As a control, a piece of 3 w/w% gelatin crosslinked with 4 w/w% MTG powder was cooked under the same conditions.

## 2.10. Statistical analysis

All statistical analysis was performed in Origin(Pro), OriginLab Corporation. All plots were made in Origin(Pro), Adobe Illustrator, and ChemDraw. To determine statistical significance, we applied a one-way or two-way ANOVA test, as specified throughout for each dataset. For each pair of samples, p values were calculated (Tukey method). Box plots were drawn with the boxes representing the 25th and 75th percent quartiles, the statistical median as the horizontal line in the box, and the mean as a square symbol; the whiskers extend to the farthest points that are not outliers.

# 3. Results

## 3.1. Edible microcarrier fabrication and characterization

In this work, our goal was to produce scalable, edible microcarriers that supported the differentiation of myoblasts into myotubes. Since myoblast proliferation and differentiation are sensitive to physical and mechanical cues [18,23–25], we sought to fabricate microcarriers with tunable stiffness and topology. For this proof-of-concept demonstration, we used gelatin as a material which enables the microcarriers to be incorporated into a final food product. Gelatin is partially hydrolyzed collagen and contributes to the desired texture and mouthfeel of meat products [55]. Importantly, gelatin hydrogels can be molded to have micron-scale surface features [36], and the gel stiffness can be tuned by modulating the polymer concentration or the degree of crosslinking [56]. To maintain microcarrier structure under culture conditions, we enzymatically crosslinked the gelatin using food-grade microbial transglutaminase (MTG) [57], which catalyzes the formation of an isopeptide bond between the  $\gamma$ -carboxamide groups of glutamine side chains and the  $\epsilon$ -amino groups of lysine side chains (Fig. 1B).

To ensure that these edible microcarriers could support the production of cultured meat, we developed a scalable fabrication strategy. We produced gelatin microparticles by generating droplets of a water-in-oil emulsion (Fig. 1A), where the dispersed phase was a gelatin solution and the continuous phase was mineral oil with Span 80 as the surfactant. The resultant gelatin microparticles were the basis for the two types of edible microcarriers used in this study: spherical microcarriers (sMCs) with a spherical shape and smooth surface topology; and grooved microcarriers (gMCs) with a disc-like shape and a grooved surface topology (Fig. 1). The stiffness of the sMCs was controlled by modulating the concentration of gelatin in the aqueous phase. After crosslinking, microcarriers were separated from the continuous phase by gradually solubilizing the oil mixture in isopropanol (Fig. 1C). After retrieving sMCs from the oil phase and fully hydrating, we observed a slight ~10% increase in diameter due to swelling (Figs. S1A and B). To obtain microcarriers with dimensions that could support suspension culture of cells in a bioreactor [27], we used a step-wise filtration process to generate three distinct populations of sMCs with median diameters of  $39 \pm 13$ ,  $87 \pm 18$ , and  $121 \pm 27$   $\mu\text{m}$  achieved by filtration between 20 and 60, 60–100, and 100–150  $\mu\text{m}$  porous membranes, respectively (Figs. 1D and Fig. 2A–C, E); this resulted in three sMC populations with median surface areas per microcarrier of  $5000 \pm 3,500$ ,  $23,900 \pm 9,100$ , and  $46,600 \pm 16,600$   $\mu\text{m}^2$  (Fig. 2G). For cellular studies, we used sMCs with ~24,000  $\mu\text{m}^2$  surface area (~87  $\mu\text{m}$  median diameter) (Fig. 2B, E); these sMCs have a radius of curvature similar to scaffolds used in previous tissue engineering applications [58,59]. We also chose this size of sMCs to ensure multiple cells per microcarrier—the spread area of C2C12 cells on flat substrates is ~1000  $\mu\text{m}^2/\text{cell}$  [60]—for maximal growth efficiency while minimizing the total volume of gelatin in the final food product. For comparison, the commercially available Cytodex 1 microcarriers, which we used as a control and were previously characterized for bovine satellite muscle cell culture [26], have a median diameter of  $186 \pm 26$   $\mu\text{m}$  and median surface area of  $109,000 \pm 28,800$   $\mu\text{m}^2$  (Fig. S1D).

Since scaffolds with grooved topology have been shown to promote myoblast proliferation, as well as myotube alignment and myogenesis [18,23], we sought to test if microcarriers with striated surface topology could enhance myoblast proliferation and myotube formation. To address this question, we developed a novel embossing technique to generate surface texture on the microcarriers, where a gelatin-in-oil emulsion was placed between two PDMS stamps during the crosslinking process (Fig. 1E–G). To establish proof-of-concept, we patterned striations with 10  $\mu\text{m}$  wide, 3  $\mu\text{m}$  deep grooves separated by 10  $\mu\text{m}$  wide gaps, which are dimensions that induce cell alignment and nuclear elongation along the groove direction [42]. Specifically, 10  $\mu\text{m}$  wide grooves have been shown to promote the formation of aligned myotubes [36]. To produce edible microcarriers with similar grooved topologies, we used an embossing process where the gelatin-in-oil emulsion droplets were placed in between two PDMS stamps that serve as grooved templates. A key innovation in this process was a partial crosslinking step prior to embossing. We empirically determined a crosslinking time that was sufficient to maintain individual microcarriers, while still enabling them to be embossed with a grooved topology. We found that when no pre-crosslinking occurred or the time of partial crosslinking was <5 min, the gelatin solution between molds showed liquid-like behavior and the droplets tended to fuse to each other, which resulted in embossed microcarriers with irregular shapes and sizes consistently larger than 1 mm in

diameter. If the time of crosslinking prior to embossing was too long, the gelatin particles became too stiff and did not emboss with defined  $10\ \mu\text{m} \times 3\ \mu\text{m}$  grooves. Given these criteria, we found that 20 min of partial pre-crosslinking was optimal for gMC fabrication. After the partial crosslinking period, the emulsion was cooled in an ice bath to slow the enzymatic crosslinking reaction and promote physical crosslinking of the gelatin; the solidified microparticles were then filtered through a  $400\ \mu\text{m}$  filter prior to embossing (see Fig. S1C for the size distribution of these filtered droplets prior to embossing). The cooled emulsion was pipetted between two PDMS stamps (Fig. 1E) that were pressed together by placing a warm ( $65\ ^\circ\text{C}$ ) acrylic block on top of the PDMS-emulsion-PDMS sandwich (Fig. 1F); this block provided a source of heat and physical force to ensure that the droplets softened, pressed into the stamps, and conformed to the grooves (Fig. 1G). After a set crosslinking time, the resultant disc-shape gMCs were released from the stamps with a pressurized stream of water. The gMCs were collected onto a  $100\ \mu\text{m}$  mesh to filter out smaller particles (Fig. 2D), which resulted in disc-shaped microcarriers with a median diameter of  $191 \pm 333\ \mu\text{m}$  (Fig. 2F) and median surface area of  $57,300 \pm 598,000\ \mu\text{m}^2$  (Fig. 2H). While the largest fraction of gMC microcarriers have  $\leq 250\ \mu\text{m}$  diameter (Fig. S1E), the bulk of the total gMC surface area is derived from gMCs with diameter  $\sim 500\text{--}1000\ \mu\text{m}$  or surface area  $\sim 400,000\text{--}1,600,000\ \mu\text{m}^2$  (Fig. S1F). We confirmed with atomic force microscopy (AFM) and confocal microscopy that the grooved topology of the PDMS stamp was successfully replicated in the gMCs with  $13.4 \pm 0.8\ \mu\text{m}$  wide and  $2.3 \pm 0.2\ \mu\text{m}$  deep parallel ridges and grooves (Fig. 2I). By comparing the groove dimensions of the PDMS stamps used to mold the gMCs, we estimated that the gMCs swell by  $\sim 30\%$  once fully hydrated. Analysis of confocal microscopy images also revealed that gMCs had an average thickness of  $20.9 \pm 6.7\ \mu\text{m}$  (Fig. 2I.iii, 2I.v).

The expansion and differentiation of precursor muscle cells is also sensitive to scaffold stiffness [24,25]. Since  $\sim 8\text{--}16\ \text{kPa}$  substrate stiffness has been shown to be optimal for the myogenesis of mouse C2C12 cells [24], we sought to fabricate microcarriers with stiffness in this range. To control the stiffness of the edible microcarriers, we varied the gelatin concentration and crosslinking time. We then characterized the mechanical properties of the microcarriers using AFM. For the sMCs, we found that the Young's modulus ( $E$ ) increased monotonically with gelatin concentration (Fig. 2J); these findings are consistent with previous reports that increasing the concentration of gelatin crosslinked with MTG results in increased hydrogel stiffness [61]. To control the stiffness of the gMCs, we tuned the crosslinking time, which we found to be a more consistent way to control gMC stiffness than changing the gelatin concentration (Fig. S2); the origins of this inconsistency are not fully understood, but could be due to dehydration of the gMCs in the PDMS molds that effectively changes the gelatin concentration of the gMCs. For the same 9 wt% gelatin formulation as the sMCs, we found that gMC stiffness increased monotonically with crosslinking time (Fig. 2J). Increasing the crosslinking time by  $\sim$  hours resulted in statistically significant increases in the Young's modulus of the gMCs. Due to the tunability of the gelatin microcarriers, we were able to produce sets of sMCs and gMCs with similar stiffnesses (Fig. 2J, Table 1). A full set of the conditions that we established to achieve microcarriers with a range of Young's moduli from  $\sim 0.5$  to  $22\ \text{kPa}$  are displayed in Table 1. For our subsequent investigations of myoblast proliferation and differentiation, we used

sMCs with  $E = 14.9$  kPa (9 wt% gelatin crosslinked for 24 h) and gMCs with  $E = 14.1$  kPa (9 wt% gelatin and crosslinked for 8 h). As a control, the commercially available Cytodex 1 microcarriers were used; these have a Young's modulus of 50 kPa [62].

### 3.2. Cell expansion on microcarriers

To investigate the potential of edible microcarriers to support the growth of myogenic tissue, we first analyzed the proliferation of mouse myogenic C2C12 cells on sMCs and gMCs. C2C12 cells provide a valuable model system to characterize myoblast differentiation into myotubes [63,64], and can thus be instructive for cultured meat applications. To evaluate the potential of sMCs and gMCs to support cell proliferation in suspension culture, cells were seeded onto microcarriers and cultured over 7 days (Fig. 3A–C). For comparison, we seeded cells on Cytodex 1 microcarriers. To ensure that the available microcarrier surface area in the cell culture volume was consistent across experiments with different types of microcarriers, we seeded cells at 11,400 cells/cm<sup>2</sup> microcarrier in 1 mL of culture. We confirmed that cells were attached to all types of microcarriers at 1, 4, and 7 days after seeding using widefield and confocal microscopy (Fig. 4A–I, Figs. S3A–I). After 1 day in culture, we found that C2C12 cells exhibited a spread morphology as indicated by the average projected spread area of cells (Fig. S3J), which is consistent with the spread area of C2C12s on flat substrates [60].

After 1 day in culture, cells on the gMCs aligned along the direction of the gMC grooves (Fig. 4B). To quantify cell alignment on gMCs, we determined the orientation angle ( $\theta$ ) of cells with respect to the gMC groove direction (Fig. 4J); this data revealed that  $\theta < 30^\circ$ , indicating that cells tended to align along the grooves after 1 day in culture, which is consistent with the contact guidance phenomenon that has been observed for various types of cells on grooved surfaces, including C2C12s [36]. Similarly, cell nuclei were aligned with the groove direction after 1 day in culture and maintained alignment after 7 days (Fig. S3K). By contrast, we observed random orientation of both cells and nuclei on sMCs and Cytodex microcarriers after 1 day and 7 days in culture (Fig. 4J; S3K).

To quantify the growth of cells on the microcarriers, we measured genomic DNA [26] (Fig. 4K). Since cells were observed to grow into the interstitial spaces between microcarriers, and may not always have been attached to a microcarrier surface, we report the cell concentration in cells/mL of bioreactor culture volume. For sMCs and gMCs, the cell density was significantly higher after 8 days of culture ( $p = 5.5 \times 10^{-4}$  for sMCs and  $p = 6.9 \times 10^{-5}$  for gMCs, d0 vs. d8 one-way ANOVA), showing that edible microcarriers supported cell proliferation (Fig. 4K). While the number of cells on the gMCs and sMCs was not significantly different at day 8 (one-way ANOVA,  $p = 0.46$ ), there was an increased number of cells on gMCs compared to sMCs at days 4 and 6 ( $p = 0.016$  at day 4,  $p = 0.010$  at day 6, one-way ANOVA). Overall, gMCs supported a larger number of cells than sMCs ( $p = 2.9 \times 10^{-5}$ ), and sMCs supported more cells than Cytodex microcarriers ( $p = 3.1 \times 10^{-5}$ ) as revealed by two-way ANOVA post-hoc multiple comparisons, suggesting that gMCs may provide an advantage for cell growth. The differences in cell proliferation on the edible microcarrier types compared to Cytodex 1 may be attributed to differences in microcarrier porosity, surface chemistry, and stiffness; all of these parameters can affect

cell growth [65]. In addition, cells on sMCs and gMCs tended to occupy volume between microcarriers over the time course of cell expansion (Fig. 4D, E, G, H); this could allow for increased cell growth compared to cells on Cytodex microcarriers (Fig. 4F, I, Figs. S3F and I). Taken together, these results show that edible microcarriers can support cell expansion in a suspension culture.

During the expansion phase, we also observed the formation of aggregates containing cells and microcarriers (Figs. 3D & Fig. 4L–N). After 1 day in culture, cells were attached between carriers in regions where microcarriers were in proximity to one another (Fig. 4A–C, Figs. S3A–C). By day 4, cells remained attached and were observed to fill in the interstitial spaces between microcarriers (Fig. 4D–F). After 7 days in culture, aggregates containing cells and sMCs had an average diameter of  $755 \pm 257$  and aggregates with cells and gMCs were  $601 \pm 169$   $\mu\text{m}$  in diameter (Fig. 4O). The aggregates did not break apart after vigorous pipetting, suggesting that cells attached to both microcarriers and other cells. By contrast, cells grown on Cytodex carriers formed smaller, aggregates with  $485 \pm 172$   $\mu\text{m}$  average diameter (Fig. 4N and O).

### 3.3. Cell differentiation on microcarriers

A major goal of cultured meat production is to generate skeletal muscle that has features of native tissue. We next explored the ability of our edible microcarriers to support the differentiation of precursor myoblasts into myotubes. To induce C2C12 myotube formation, we replaced the growth medium with differentiation induction media after 7 days of expansion. To confirm myoblast differentiation, we visualized DNA, F-actin, and the myogenic marker myosin heavy chain 4 (Myh4) in microtissues by confocal microscopy. Consistent with skeletal muscle formation [66], we observed increased fluorescence intensity of immunolabeled Myh4, indicating increased expression at the protein level (Fig. 5A–C). Widefield imaging revealed that cells maintained coverage over the sMCs and gMCs during the 7 day differentiation time course (Fig. 5A.i, B.i, Figs. S4A–F). Reconstructed 3D confocal images of the sMC (Fig. 5A.ii and A.iii) and gMC (Fig. 5B.ii and B.iii) microtissues revealed prominent, elongated, multinucleated myotubes that were interwoven throughout the microtissues, spanning multiple microcarriers and showing strong Myh4 expression. We observed myotubes that spanned across the surface (Fig. 5A.iv and B.iv) and into the interior (Fig. 5A.v and B.v) of the sMC and gMC microtissues, a characteristic that was not observed on Cytodex microcarriers (Fig. 5C.iv–v). By contrast, Myh4-positive, multinucleated structures were more rounded and did not span across multiple Cytodex microcarriers (Fig. 5C.ii and C.iii). In addition, we observed that many of the Cytodex 1 microcarriers were free of cells with the cells aggregated together and Cytodex microcarriers on the periphery (Fig. 5C.i and C.ii, Figs. S4G–I), which has been observed previously for mesenchymal cells on Cytodex 1 microcarriers [67]. Similar cell detachment leaving denuded regions of glass and cellulose microcarriers has also been observed after the initial growth of C2C12 cells [28,68]. While myotubes have been shown to form and bridge across multiple Cytodex 3 microcarriers—similar to our observations of myotubes in sMC and gMC microtissues—Cytodex 3 microcarriers are coated with gelatin and have a different surface chemistry than Cytodex 1, suggesting that myotube formation may be sensitive to the type of microcarrier.

Because myofibrils are a prominent feature of skeletal muscle, myotubes are considered a desired component of cultured meat. We thus next quantified the length and density of myotubes in the microtissues. We found that within the 3D volume of the microtissues, the average length of myotubes was  $118 \pm 63 \mu\text{m}$  (sMC),  $126 \pm 58 \mu\text{m}$  (gMC), and  $32 \pm 19 \mu\text{m}$  (Cytodex) (Fig. 5D). The myotube lengths in sMC and gMC microtissues were not significantly different ( $p = 0.65$ ) but were longer than myotubes on Cytodex microcarriers ( $p < 10^{-3}$ ). To quantify the volume fraction of different components of the microtissues, we applied a machine learning technique that classified the 3D confocal images on a voxel-by-voxel basis into one of five categories: nucleus, gelatin microcarrier, myotube, F-actin, and background; we then calculated the volume fraction that was occupied by myotubes. We found that myotubes accounted for  $39 \pm 13\%$  (sMCs),  $33 \pm 7\%$  (gMCs), and  $7 \pm 6\%$  (Cytodex) of the cellular volume component of microtissues (Fig. 5E), showing that edible microcarriers supported a significantly higher myotube fraction than the Cytodex carriers ( $p < 10^{-3}$ ). We observed no statistical difference in the myotube fraction between sMC and gMC microtissues ( $p = 0.50$ ), indicating that both microcarrier types equivalently support myotube production.

To quantify cellular alignment in microtissues, which is another important feature of skeletal muscle, we examined the alignment of F-actin in microtissues (Fig. S5). At length scales of a single cell, F-actin alignment can be an indicator of cellular elongation or stress fiber formation [53,54], and at length scales of myotubes, F-actin alignment correlates with myotube alignment [69], which is a key feature of skeletal muscle. To quantify F-actin alignment, we calculated a parameter termed the orientation index (OI) that is derived from the Fourier transform power spectrum of images to quantify actin alignment at different length scales: as actin alignment increases,  $\text{OI} \rightarrow 100$ ; as the fiber network becomes more diffuse and randomly oriented,  $\text{OI} \rightarrow 0$ . At subcellular length scales ( $1.60\text{--}3.51 \mu\text{m}$ ) we found that there was no significant difference in the F-actin alignment between the three microcarrier types (Fig. 5F). However, at length scales from  $\sim 7 \mu\text{m}$ , which is on the length scale of a single cell, up to  $\sim 64 \mu\text{m}$  which approaches the length scale of myotubes, there is significantly increased alignment of actin in cells grown on sMCs and gMCs rather than Cytodex, which is consistent with increased myotube production in edible microtissues (1-way ANOVA:  $p < 10^{-3}$  at both  $6.71$  and  $64.0 \mu\text{m}$  length scales) (Fig. 5F). For images of the cells on Cytodex microcarriers, the OI could not be quantified for regions  $>65 \mu\text{m}$  since the aggregates were not consistently large enough (Fig. 5C.i and C.ii).

To further characterize the microtissues, we assessed nuclear shape by determining the nuclear major-to-minor axis ratio (Fig. S6A). The nuclear major-to-minor axis ratio is sensitive to cellular morphology, external strain, and intracellular tension, with more elongated nuclei reflecting increased cellular tension and/or elongation [70,71]. Our findings reveal that cells on gMCs and sMCs had a larger major-to-minor axis ratio, as they were more elliptical, which is also consistent with the elongation of cells and/or increased cellular tension on gMCs and sMCs. By contrast, cells on Cytodex microcarriers had a smaller major-to-minor axis ratio, which may suggest they were that they are under less anisotropic strain or experiencing less cellular tension.

Another major goal in cultured meat production is to generate tissues with cell densities of  $\sim 10^8$  cells/cm<sup>3</sup>, which have been shown to be optimal for generating functional human skeletal muscle [17]. To measure the density of cells in the microtissues we applied an object classification algorithm to analyze the confocal images. Because myotubes tended to be larger than the imaging window, we reported the density of nuclei in microtissues as a metric for the density of cellular matter. This analysis revealed on the order of  $10^8$  nuclei/cm<sup>3</sup> within both sMC and gMC microtissues (Fig. 5G), which is slightly higher than the density of nuclei in murine muscle fibers of  $\sim 2\text{--}7 \times 10^7$  nuclei/cm<sup>3</sup> [72]. For mononucleated cells, the same density of  $10^8$  nuclei/cm<sup>3</sup> that we observed in sMC and gMC microtissues translates to a cell density of  $10^8$  cells/cm<sup>3</sup>, which is slightly lower than typical animal tissue ( $\sim 1\text{--}3 \times 10^9$  cells/cm<sup>3</sup>) [73] and other 3D tissue constructs and spheroids composed of mononucleated cells ( $\sim 1\text{--}8 \times 10^9$  cells/cm<sup>3</sup>) [74,75]. To compare the density of nuclei in the sMC and gMC microtissues to cells on the inedible Cytodex microcarriers, we also quantified the nuclear density within the cell matter-only component of the microtissues (cell volume excluding microcarriers) (Fig. S6B). We found that microcarrier type did not significantly impact the density of nuclei in the microtissue cellular matter component. Since microcarrier scaffolds could impact the texture of the final meat product, we also quantified the microtissue volume that was occupied with edible microcarrier. We found that the microcarriers comprised  $46 \pm 13$  vol% of the sMC and  $35 \pm 18$  vol% of the gMC microtissues, with the rest being filled by cellular matter (nuclei, cell body, myotubes) (Fig. 5H). Microcarrier volume estimates were not performed for the Cytodex microcarriers since they were not integrated within the microtissue but rather at the periphery of the cellular aggregate. Since the efficiency of myotube differentiation on Cytodex microcarriers was poor, we focused subsequent analyses on edible sMC and gMC myogenic microtissues.

To further characterize edible myogenic microtissues, we measured *Myh4* and myocyte-specific enhancer factor 2C (*Mef2c*) transcripts in differentiated C2C12 microtissues using RT-qPCR after culturing in differentiation induction media for 7 days. Cells on both types of edible microcarriers showed equivalent  $\sim 10^2\text{--}10^4$ -fold increases in *Mef2c* and *Myh4* expression over undifferentiated cells grown on tissue culture plastic ( $p < 0.0001$ ) (Fig. 6); this increase was statistically similar to cells differentiated on tissue culture plastic. These findings indicate that both sMC and gMC edible microcarriers support myoblast differentiation as sufficiently as typical C2C12 differentiation conditions.

#### 3.4. Edible microcarriers support proof-of-concept cultured bovine meat

To investigate the ability of the edible microcarriers to support the generation of cultured meat, we cultured bovine satellite muscle cells (BSMCs) on sMCs in a 100 mL spinner flask (Fig. 7A), which is commonly used to test the scale-up of cell culture [27]. Since sMCs can be readily fabricated at larger quantities and had similar microtissue characteristics to gMCs (Fig. 5), we focused this proof-of-concept scale-up on BSMCs cultured on sMCs. Cells were expanded on sMCs for 7 days before inducing differentiation for an additional 7 days. Consistent with our observations of C2C12 cells cultured with edible microcarriers in smaller volume suspension cultures, we found that BSMCs and microcarriers spontaneously formed into microtissues (Fig. 7B, Fig. S7A). To harvest the microtissues and form a consolidated cultured meat patty, microtissues were centrifuged and mixed with gelatin (3



wt %) and MTG powder (4 wt%), which promoted the formation of a cohesive piece of cultured meat (Fig. 7C and D, Supp Figs. S7B and C). To evaluate cookability, we placed the cultured meat on a ~195 °C hot plate with olive oil until browned (Fig. 7E, Figs. S7D–F). Upon heating, the cultured meat patty retained its shape (Fig. 7E); by contrast, the control gelatin samples melted and lost their form, consistent with the phase behavior of gelatin hydrogels (Figs. S6G–I, Video S1). The BSMC-cultured meat also exhibited browning, characteristic of Maillard reactions (See Fig. 7E). After cooking, the patty could be cut into pieces, which also held their form, reflecting the solid-like properties of the microtissue-based meat (Video S2). These proof-of-concept findings show that edible microcarriers support BSMC culture in a stirred-flask bioreactor and the generation of cookable bovine cultured meat. In this proof-of-concept demonstration using 100 mL spinner flask and a microcarrier density of 8.8 cm<sup>2</sup>/mL, we were able to produce 2.9 g of cultured meat. Assuming a linear scaling with culture volume, a back-of-the-envelope calculation estimates that 1 kg of meat could be produced in a ~40 L bioreactor. We note that the concentration of microcarriers could be tripled in optimized conditions and additional media feed or gas exchange could improve cell growth efficiency [27].

Supplementary video related to this article can be found at <https://doi.org/10.1016/j.biomaterials.2022.121669>.

#### 4. Discussion

Cultured meat has potential to provide a complementary approach for animal protein production, but strategies to scale up cultured meat production will be critical. To increase the efficiency of cultured meat growth, edible scaffolds [32]—including fibrous gelatin [34] and textured soy protein [33]—have promise, but need to be compatible with larger scale suspension culture in a bioreactor for maximum impact. Here we show a scalable approach to generate edible microcarriers that support the production of myogenic microtissues in a single stirred-flask bioreactor. After differentiation, the microtissues could be harvested into a cookable cultured meat patty.

In defining a process to fabricate edible microcarriers that are optimized for myoblast culture and differentiation, we used gelatin as a microcarrier material based on the following rationale: 1) the mechanical properties of gelatin microcarriers can be easily tuned; 2) gelatin microcarriers can be embossed by crosslinking the hydrogels in a predefined mold; 3) gelatin promotes cell attachment as it derives from the common ECM protein collagen and inherently contains cell binding domains so no further chemical modifications with tailored peptides are required; 4) production of gelatin microcarriers can be achieved using existing food-grade materials; and 5) gelatin contributes to positive sensory attributes of meat including taste, mouthfeel, and texture, as well as nutritional properties [55]. While we demonstrate this proof-of-concept methodology using gelatin, edible microcarriers could be fabricated using other plant-based scaffolding materials [31] or non-animal sources of gelatin [76], which may be desired for cultured meat applications. The fabrication of alginate, agarose, and pectin microbeads using emulsions as templates has been previously described in the literature by our group and others [41,77–80] and is similar to the process we describe here to produce edible microcarriers. Since materials used for scaffolds can

positively contribute to sensory attributes of processed meat products [81], it will be interesting in future work to explore how modulating scaffold texture—either by altering the polymer type, concentration, or crosslink density—could enhance final meat texture.

We envision that the embossing technique that we developed to produce gMCs with aligned surface topology gMCs can be modified to further advance fundamental research of edible microcarriers for cultured meat production. The microcarrier groove width and height can be easily tuned using standard approaches in soft lithography. The microcarrier thickness can be modulated by using spacers with different thickness, and the size of the gMCs can be modified by filtering the emulsion prior to embossing. Modulating gMC size and shape could impact their dispersion and sedimentation in a suspension culture. For example, microcarriers with a smaller size sediment more slowly [27], and microcarrier shape and aspect ratio could be tuned to modulate their dispersion and sedimentation in solution [82]. Further experiments and mathematical modeling will need to be performed to fully understand how differently shaped microcarriers disperse in solution and aggregate during cell expansion in a bioreactor context.

While our study of microcarriers with grooved topology was motivated to test if grooved topologies could promote myoblast proliferation and myotube formation in a bioreactor context, we found that both sMC and gMC edible microcarriers support the attachment, proliferation, and myotube formation of C2C12 cells. While the number of cells on gMCs and sMCs was similar after 8 days, we found that the overall expansion on gMCs was modestly higher on gMCs than on sMCs. We observed a slight increase in proliferation for C2C12 cells on gMCs compared to sMCs at initial time points; an observation which is consistent with findings that C2C12 growth is faster on topologically aligned surfaces [23]. Since any reductions in culture time could have major impact on cost and production efficiency, strategies to optimize the doubling time and expansion potential of muscle satellite cells are currently an intense focus in the field [83]. Future studies should more fully explore the effects of microcarrier surface topology on cell expansion.

While myotube formation is dependent on the physical and mechanical properties of the surrounding microenvironment [24], we found that both sMC and gMC edible microcarriers supported myogenic differentiation and the formation of myotubes that were  $\sim 10^2$   $\mu\text{m}$  in length. We observed alignment of myoblasts with the gMC grooves during the expansion phase, but the myotubes that formed with differentiation did not tend to follow the original grooved striations of the gMCs but rather spanned across the interstitial spaces between microcarriers; the alignment of F-actin after differentiation was also equivalent for sMC and gMC microtissues. In addition, we did not find any significant advantages of the gMC over the sMC microtissues in terms of myotube volume fraction, myotube length, expression of myogenic markers, or density of nuclei in microtissues. To further characterize muscle development on edible microcarriers at different stages of differentiation, other proteins such as desmin, MyoD, and myogenin could be targeted [84]. Taken together, these findings demonstrate the potential of both sMC and gMC edible microcarriers to support the scalable production of myotubes—which are the basis of skeletal muscle tissue—from naturally adherent myoblasts in a bioreactor. These results will also be important to guide future strategies in cultured meat production, since aligned nanofiber sheets and scaffolds with

striated texture have been considered top contenders to produce cultured meat due to their demonstrated effects on increasing myogenic potential [85]. Beyond the scope of this paper, elucidating the biological mechanisms underlying the effects of microcarrier stiffness and surface topology on the proliferation and differentiation of myogenic cells in suspension culture will be an important topic of future investigations, for example, to map the effects of physical and mechanical scaffold cues on cell behaviors in the presence of additional physical forces due to fluid flow.

Considering how production of sMCs can be scaled simply by increasing vessel size, sMCs have strong potential as an efficient approach for scaling up muscle microtissue production. By contrast, the laboratory-scale fabrication method for gMCs that we present here requires roughly an order of magnitude more time to prepare an equivalent yield of sMCs and we found that microcarriers with grooved topologies do not provide significant advantages over sMCs for C2C12 cell expansion or myogenesis. While we did observe a modest increase in proliferation for cells on gMCs in the initial days of expansion, the potential benefits of microcarrier surface texture for cell proliferation could be explored more efficiently with production of microcarriers with defined surface topology using industrial-scale methods [86]; this may alter the cost-benefit analysis of culturing meat using grooved microcarriers. Microcarriers with micron-scale surface texture could also be generated using methods including extrusion, photopatterning, microfluidics, or random surface wrinkling [87–94]. In addition, edible microcarriers with grooved topology could benefit other desired phenotypes for cultured meat applications. For example, textured scaffolds have been shown to increase lipid accumulation in adipocytes [95] and could therefore have potential to accelerate adipose tissue production for enhanced flavor and sensory properties of cultured meat. Grooved microcarriers could also positively impact the final textural and sensory properties of cultured meat; the higher surface area to volume ratio of these microcarriers could accelerate their enzymatic degradation. Beyond cultured meat, microcarriers with tunable topology and stiffness could have applications for other systems where large-scale cultured of cells is needed, including but not limited to cell culture for immunotherapies [96], neural engineering [97], and fibroblast reprogramming for regenerative medicine applications [42].

The scalable fabrication strategy that we developed to produce edible microcarriers is compatible with ingredients and processes already used in food production. Since common reagents to chemically crosslink protein-based hydrogels, such as glutaraldehyde and 1-ethyl-3-(3'-dimethylaminopropyl)carbodiimide (EDC) [98], are not appropriate for food products, we focused on developing edible microcarriers using reagents that are already accepted in the food industry. To generate edible microcarriers, we produced hydrogel microparticles using droplets of a water-in-oil emulsions, which is a scalable technique already used in industrial applications, including in the food space [99–102]. Investigating the long-term storage of edible microcarriers will be important for future commercial applications. While gelatin-based hydrogels can be dehydrated after production and rehydrated before use, additional experiments need to be performed to determine how dehydration conditions affect microcarrier size, surface roughness, mechanical properties, and density, which are important characteristics that can regulate cellular behaviors that are important for cultured meat, including proliferation and differentiation.

The scale-up of edible microtissue production in a bioreactor will also require additional optimization. While the viability of cells in edible microtissue aggregates with diameter  $>500\ \mu\text{m}$  could be impacted due to diffusion-limited exchange of nutrients and oxygen between cells and media—estimates of the maximum thickness of viable tissue that can be maintained by media diffusion are comparable to the size of our microtissue aggregates—these estimates are for static conditions [12, 103] and media exchange is enhanced by fluid flow in a bioreactor context [104]. Furthermore, some studies have suggested that hypoxic conditions can accelerate myoblast proliferation and do not negatively impact differentiation [105,106]. Still, microcarrier aggregation can be countered by using strategies such as increasing bioreactor spin speeds or decreasing the initial seeding density during inoculation [27]. Considering that microtissue size and impact on cell viability will ultimately depend on various factors including bioreactor geometry, fluid flow rates, porosity of edible microcarriers, and the metabolic rate of cells [27], further studies will be necessary to evaluate media exchange in the context of scaled-up cultured meat production.

The formation of edible microtissues that we observed during the expansion phase have potential to support many desired features of cultured meat. Since the cells within the edible microtissues occupy the interstitial spaces between microcarriers, we achieved densities of nuclei in microtissue that are consistent with cell density goals of cultured meat ( $\sim 10^7$ - $10^8$  cells/ $\text{cm}^3$ ) [17,19,29]. While the nuclear density in muscle tissue cannot be directly comparable to cell density given that muscle cells are multinucleated, our findings are in the range of previous reports of  $\sim 2$ – $7 \times 10^7$  nuclei per  $\text{cm}^3$  of murine muscle fibers [72] and  $\sim 2 \times 10^5$  muscle fibers per  $\text{cm}^3$  of muscle [72]. We also found that the microcarrier volume fraction of the microtissues was  $\sim 35$ – $45$  vol%, with the remaining volume filled by cellular matter including myotubes and undifferentiated myoblasts ( $55$ – $65$  vol% cellular matter); by comparison, muscle fibers comprise  $\sim 60$ – $70$ % of bovine muscle tissue [107]. In future iterations of this work, we expect that increasing the surface area-to-volume ratio of the microcarriers could enable us to achieve higher cell densities in the microtissues. Alternatively, we could explore increasing the enzymatic or hydrolytic degradation rate of the microcarriers with the goal of accelerating decomposition of the microcarriers, hence, decreasing the fraction of the microtissues occupied by microcarrier and increasing the volume fraction of myotubes. Understanding the degradation behavior of gelatin-based microcarriers and ECM remodeling in the context of bidirectional mechanical feedback between cells and the matrix will also be important especially with respect to the final texture of the cultured meat [108].

Microtissues with edible microcarriers have several attractive features in the context of cultured meat, but there are still many challenges to tackle before cultured meat can be a delicious and sustainable protein alternative. While we found that edible microcarriers supported greater alignment of myotubes compared to Cytodex microcarriers, the alignment of myotubes in edible microtissues still does not approach the striking alignment of muscle fibers in skeletal muscle [109]. The edible myogenic microtissues showed myotubes with lengths  $\sim 100\ \mu\text{m}$ ; by comparison, typical muscle fiber length in mice is  $4$ – $6$  mm [72]. Varying culture conditions could be explored to achieve microtissues that better mimic real skeletal muscle, but it will be important to first determine how myotubes and the degree of myotube alignment contribute to cultured meat texture and flavor [110]. This

proof-of-concept demonstration shows that microtissues formed with edible microcarriers can be harvested into a cultured meat patty that evokes a product similar to ground meat. We demonstrate that edible microcarriers support the generation of murine and bovine myogenic microtissues, indicating that the approach is translatable to edible cell types. While our initial observations show the promise of edible microcarriers to support a cookable cultured bovine meat product that exhibits browning, future studies will be needed to fully assess the sensory and nutritional properties of cultured meat produced with edible microcarriers. Since animal proteins provide a complete profile of essential amino acids as well as high bioavailability and digestibility [111], we anticipate that cultured meat has potential to provide similar nutritional qualities. The taste and texture of cultured meat are key concerns of future consumers [12], and will be a major focus of future efforts in developing cultured meat production methods to tune flavor molecules that are known to be important contributors to meat flavor including 2-nonenal (grassy), 2, 4-decadienal (fatty), *trans*-4,5-epoxy-(E)-2-decenal (metallic), 1-octen-3-one (metallic), as well as myoglobin and hemoglobin [112]. The cost of cultured meat is another major focus of research efforts across the industry. In this study we cultured cells using animal serum, which is a major contributor to the cost of cultured meat production and therefore a major target for innovations to scale up production of cultured meat. Since cell proliferation and adhesion are sensitive to growth factors contained in serum, future work should evaluate combinations of edible microcarriers with serum-free media, which could further optimize process efficiency. Functionalizing the surface of the microcarriers with specific growth factors or signaling compounds could be explored to further increase muscle growth efficiency. Ultimately, microtissues with edible microcarriers could provide the basis for a delicious cultured steak, which has the longer-range structure that could be achieved by patterning muscle and adipose microtissues.

## 5. Conclusions

In summary, we present here edible microcarriers that can support the generation of bovine and murine myogenic microtissues in suspension culture. While we explored the grooved topology of edible microcarriers as a strategy to promote myogenic microtissue production, we found largely equivalent effects of sMCs and gMCs on cell growth, differentiation. The scalable approach that we describe to generate edible microcarriers and the resultant muscle microtissues has potential to contribute to efficient, cost-effective cultured meat production, which could provide a complementary alternative for animal protein production that ultimately could help to increase the resilience of future food systems.

## Supplementary Material

Refer to Web version on PubMed Central for supplementary material.

## Acknowledgements

The authors acknowledge the use of instruments at the Nano & Pico Characterization Lab at the California NanoSystems Institute and the MCDB/BSCRC Microscopy Core. We thank the lab of Professor Song Li, UCLA Bioengineering, for providing the silicon wafer molds. We are grateful to the Kaplan lab at Tufts University for generously providing the bovine satellite muscle cells and to Jessica Castillo of the NIH National Center

for Advancing Translational Sciences UCLA Clinical and Translational Science Institute (UL1TR001881) for the expert support with graphic illustrations.

### Funding

This work was supported by the United States Department of Agriculture National Institute of Food and Agriculture, AFRI project CALW-2021-09608; the Good Food Institute; the New Harvest Foundation (Fellowship to NSK and Seed Grant to ARD); the National Science Foundation Innovations at the Nexus of Food, Energy, and Water Systems (INFEWS) training grant (DGE-1735325, which supported NSK & KC); a National Science Foundation Boosting Research Ideas for Transformative and Equitable Advances in Engineering (BRITE) Fellow Award (to ACR, CMMI-2135747); and the UCLA California NanoSystems Institute and the Noble Family Innovation Fund. SCPN was supported by the National Institute of Dental & Craniofacial Research of the National Institutes of Health under Award Number F32DE030004.

### Data availability

Data will be made available on request.

### References

- [1]. Karimi V, Karami E, Keshavarz M, Vulnerability and adaptation of livestock producers to climate variability and change, *Rangel. Ecol. Manag.* 71 (2018) 175–184, 10.1016/j.rama.2017.09.006.
- [2]. Westhoek H, Lesschen JP, Rood T, Wagner S, De Marco A, Murphy-Bokern D, Leip A, van Grinsven H, Sutton MA, Oenema O, Food choices, health and environment: effects of cutting Europe's meat and dairy intake, *Global Environ. Change* 26 (2014) 196–205, 10.1016/j.gloenvcha.2014.02.004.
- [3]. Nijdam D, Rood T, Westhoek H, The price of protein: review of land use and carbon footprints from life cycle assessments of animal food products and their substitutes, *Food Pol.* 37 (2012) 760–770, 10.1016/j.foodpol.2012.08.002.
- [4]. Eshel G, Shepon A, Makov T, Milo R, Land, irrigation water, greenhouse gas, and reactive nitrogen burdens of meat, eggs, and dairy production in the United States, *Proc. Natl. Acad. Sci. U. S. A.* 111 (2014) 11996–12001, 10.1073/pnas.1402183111. [PubMed: 25049416]
- [5]. Steinfeld H, Gerber P, Wassenaar T, Castel V, Rosales M, de Haan C, *Livestock's Long Shadow: Environmental Issues and Options*, Food and Agriculture Organisation of the United Nations, 2006.
- [6]. Biggs R, Schlüter M, Schoon Michael L. (Eds.), *Principles for Building Resilience: Sustaining Ecosystem Services in Social-Ecological Systems*, Cambridge University Press, 2015.
- [7]. Slade P, If you build it, will they eat it? Consumer preferences for plant-based and cultured meat burgers, *Appetite* 125 (2018) 428–437, 10.1016/j.appet.2018.02.030. [PubMed: 29501683]
- [8]. Verbeke W, Pérez-Cueto FJA, de Barcellos MD, Krystallis A, Grunert KG, European citizen and consumer attitudes and preferences regarding beef and pork, *Meat Sci.* 84 (2010) 284–292, 10.1016/j.meatsci.2009.05.001. [PubMed: 20374787]
- [9]. Tuomisto HL, Teixeira de Mattos MJ, Environmental impacts of cultured meat production, *Environ. Sci. Technol.* 45 (2011) 6117–6123, 10.1021/es200130u. [PubMed: 21682287]
- [10]. Mattick CS, Landis AE, Allenby BR, Genovese NJ, Anticipatory life cycle analysis of in vitro biomass cultivation for cultured meat production in the United States, *Environ. Sci. Technol.* 49 (2015) 11941–11949, 10.1021/acs.est.5b01614. [PubMed: 26383898]
- [11]. Odegard I, Sinke P, LCA of Cultivated Meat, Future projections for different scenarios, 2021.
- [12]. Tomiyama AJ, Kawecki NS, Rosenfeld DL, Jay JA, Rajagopal D, Rowat AC, Bridging the gap between the science of cultured meat and public perceptions, *Trends Food Sci. Technol.* 104 (2020) 144–152, 10.1016/j.tifs.2020.07.019.
- [13]. Kwee BJ, Mooney DJ, Biomaterials for skeletal muscle tissue engineering, *Curr. Opin. Biotechnol.* 47 (2017) 16–22, 10.1016/j.copbio.2017.05.003. [PubMed: 28575733]
- [14]. Bach AD, Beier JP, Stern-Staeter J, Horch RE, Skeletal muscle tissue engineering, *J. Cell Mol. Med.* 8 (2004) 413–422, 10.1111/j.1582-4934.2004.tb00466.x. [PubMed: 15601570]

- [15]. DiEdwardo CA, Petrosko P, Acarturk TO, DiMilla PA, LaFramboise WA, Johnson PC, Muscle tissue engineering, *Clin. Plast. Surg.* 26 (1999) 647–656, 10.1016/S0094-1298(20)32663-8. [PubMed: 10553219]
- [16]. Costantini M, Testa S, Mozetic P, Barbetta A, Fuoco C, Fornetti E, Tamiro F, Bernardini S, Jaroszewicz J, wi szkowski W, Trombetta M, Castagnoli L, Seliktar D, Garstecki P, Cesareni G, Cannata S, Rainer A, Gargioli C, Microfluidic-enhanced 3D bioprinting of aligned myoblast-laden hydrogels leads to functionally organized myofibers in vitro and in vivo, *Biomaterials* 131 (2017) 98–110, 10.1016/j.biomaterials.2017.03.026. [PubMed: 28388499]
- [17]. Kim JH, Seol YJ, Ko IK, Kang HW, Lee YK, Yoo JJ, Atala A, Lee SJ, 3D bioprinted human skeletal muscle constructs for muscle function restoration, *Sci. Rep.* 8 (2018) 1–15, 10.1038/s41598-018-29968-5. [PubMed: 29311619]
- [18]. Huang NF, Patel S, Thakar RG, Wu J, Hsiao BS, Chu B, Lee RJ, Li S, Myotube assembly on nanofibrous and micropatterned polymers, *Nano Lett.* 6 (2006) 537–542, 10.1021/nl060060o. [PubMed: 16522058]
- [19]. Bodiou V, Moutsatsou P, Post MJ, Microcarriers for upscaling cultured meat production, *Front. Nutr.* 7 (2020) 1–16, 10.3389/fnut.2020.00010. [PubMed: 32039228]
- [20]. Velleman S, The role of the extracellular matrix in skeletal muscle development, *Poultry Sci.* 78 (1999) 778–784, 10.1093/ps/78.5.778. [PubMed: 10228976]
- [21]. Urciuolo A, Quarta M, Morbidoni V, Gattazzo F, Molon S, Grumati P, Montemurro F, Tedesco FS, Blaauw B, Cossu G, Vozzi G, Rando TA, Bonaldo P, Collagen VI regulates satellite cell self-renewal and muscle regeneration, *Nat. Commun.* 4 (2013) 1964, 10.1038/ncomms2964. [PubMed: 23743995]
- [22]. Thomas K, Engler AJ, Meyer GA, Extracellular matrix regulation in the muscle satellite cell niche, *Connect. Tissue Res.* 56 (2015) 1–8, 10.3109/03008207.2014.947369. [PubMed: 25047058]
- [23]. Cooper A, Jana S, Bhattarai N, Zhang M, Aligned chitosan-based nanofibers for enhanced myogenesis, *J. Mater. Chem.* 20 (2010) 8904, 10.1039/c0jm01841d.
- [24]. Engler AJ, Myotubes differentiate optimally on substrates with tissue-like stiffness: pathological implications for soft or stiff microenvironments, *J. Cell Biol.* 166 (2004) 877–887, 10.1083/jcb.200405004. [PubMed: 15364962]
- [25]. Gilbert PM, Havenstrite KL, Magnusson KEG, Sacco A, a Leonardi N, Kraft P, Nguyen NK, Thrun S, Lutolf MP, Blau HM, Substrate elasticity regulates skeletal muscle stem cell self-renewal in culture, *Science* 329 (2010) 1078–1081, 10.1126/science.1191035, 80. [PubMed: 20647425]
- [26]. Verbruggen S, Luining D, van Essen A, Post MJ, Bovine myoblast cell production in a microcarriers-based system, *Cytotechnology* 70 (2018) 503–512, 10.1007/s10616-017-0101-8. [PubMed: 28470539]
- [27]. Microcarrier Cell Culture, Principles and Methods. GE Healthcare Handbook No. 18–1140-62, 2005.
- [28]. Bardouille C, Lehmann J, Heimann P, Jockusch H, Growth and differentiation of permanent and secondary mouse myogenic cell lines on microcarriers, *Appl. Microbiol. Biotechnol.* 55 (2001) 556–562, 10.1007/s002530100595. [PubMed: 11414320]
- [29]. Allan SJ, De Bank PA, Ellis MJ, Bioprocess design considerations for cultured meat production with a focus on the expansion bioreactor, *Front. Sustain. Food Syst.* 3 (2019), 10.3389/fsufs.2019.00044.
- [30]. Modulevsky DJ, Lefebvre C, Haase K, Al-Rekabi Z, Pelling AE, Apple derived cellulose scaffolds for 3D mammalian cell culture, *PLoS One* 9 (2014), e97835, 10.1371/journal.pone.0097835. [PubMed: 24842603]
- [31]. Campuzano S, Pelling AE, Scaffolds for 3D cell culture and cellular agriculture applications derived from non-animal sources, *Front. Sustain. Food Syst* 3 (2019) 1–9, 10.3389/fsufs.2019.00038.
- [32]. Ben-Arye T, Levenberg S, Tissue engineering for clean meat production, *Front. Sustain. Food Syst.* 3 (2019) 1–19, 10.3389/fsufs.2019.00046.

- [33]. Ben-Arye T, Shandalov Y, Ben-Shaul S, Landau S, Zagury Y, Ianovici I, Lavon N, Levenberg S, Textured soy protein scaffolds enable the generation of three-dimensional bovine skeletal muscle tissue for cell-based meat, *Nat. Food.* 1 (2020) 210–220, 10.1038/s43016-020-0046-5.
- [34]. MacQueen LA, Alver CG, Chantre CO, Ahn S, Cera L, Gonzalez GM, O'Connor BB, Drennan DJ, Peters MM, Motta SE, Zimmerman JF, Parker KK, Muscle tissue engineering in fibrous gelatin: implications for meat analogs, *NPJ Sci. Food* 3 (2019) 1–12, 10.1038/s41538-019-0054-8. [PubMed: 31304273]
- [35]. Kang D-H, Louis F, Liu H, Shimoda H, Nishiyama Y, Nozawa H, Kakitani M, Takagi D, Kasa D, Nagamori E, Irie S, Kitano S, Matsusaki M, Engineered whole cut meat-like tissue by the assembly of cell fibers using tendon-gel integrated bioprinting, *Nat. Commun.* 12 (2021) 5059, 10.1038/s41467-021-25236-9. [PubMed: 34429413]
- [36]. Bettadapur A, Suh GC, Geisse NA, Wang ER, Hua C, Huber HA, Viscio AA, Kim JY, Strickland JB, McCain ML, Prolonged culture of aligned skeletal myotubes on micromolded gelatin hydrogels, *Sci. Rep.* 6 (2016) 1–14, 10.1038/srep28855. [PubMed: 28442746]
- [37]. Kimura Y, Ozeki M, Inamoto T, Tabata Y, Adipose tissue engineering based on human preadipocytes combined with gelatin microspheres containing basic fibroblast growth factor, *Biomaterials* 24 (2003) 2513–2521, 10.1016/S0142-9612(03)00049-8. [PubMed: 12695078]
- [38]. Kawai K, Suzuki S, Tabata Y, Ikada Y, Nishimura Y, Accelerated tissue regeneration through incorporation of basic fibroblast growth factor-impregnated gelatin microspheres into artificial dermis, *Biomaterials* 21 (2000) 489–499, 10.1016/S0142-9612(99)00207-0. [PubMed: 10674814]
- [39]. Nawong S, Oonsivilai R, Boonkerd N, Truelstrup Hansen L, Entrapment in food-grade transglutaminase cross-linked gelatin–maltodextrin microspheres protects *Lactobacillus* spp. during exposure to simulated gastro-intestinal juices, *Food Res. Int.* 85 (2016) 191–199, 10.1016/j.foodres.2016.04.041. [PubMed: 29544835]
- [40]. Duffy DC, McDonald JC, Schueller OJA, Whitesides GM, Rapid prototyping of microfluidic systems in poly(dimethylsiloxane), *Anal. Chem.* 70 (1998) 4974–4984, 10.1021/ac980656z. [PubMed: 21644679]
- [41]. Nyberg KD, Hu KH, Kleinman SH, Khismatullin DB, Butte MJ, Rowat AC, Quantitative deformability cytometry: rapid, calibrated measurements of cell mechanical properties, *Biophys. J.* 113 (2017) 1574–1584, 10.1016/j.bpj.2017.06.073. [PubMed: 28978449]
- [42]. Downing TL, Soto J, Morez C, Houssin T, Fritz A, Yuan F, Chu J, Patel S, Schaffer DV, Li S, Biophysical regulation of epigenetic state and cell reprogramming, *Nat. Mater.* 12 (2013) 1154–1162, 10.1038/nmat3777. [PubMed: 24141451]
- [43]. Mott PH, Roland CM, Limits to Poisson's ratio in isotropic materials, *Phys. Rev. B* 80 (2009), 132104, 10.1103/PhysRevB.80.132104.
- [44]. Stringer C, Wang T, Michaelos M, Pachitariu M, Cellpose: a generalist algorithm for cellular segmentation, *Nat. Methods* 18 (2021) 100–106, 10.1038/s41592-020-01018-x. [PubMed: 33318659]
- [45]. Elter P, Weihe T, Lange R, Gimsa J, Beck U, The influence of topographic microstructures on the initial adhesion of L929 fibroblasts studied by single-cell force spectroscopy, *Eur. Biophys. J.* 40 (2011) 317–327, 10.1007/s00249-010-0649-0. [PubMed: 21153809]
- [46]. Cerqueira MT, Pirraco RP, Santos TC, Rodrigues DB, Frias AM, Martins AR, Reis RL, Marques AP, Human adipose stem cells cell sheet constructs impact epidermal morphogenesis in full-thickness excisional wounds, *Biomacromolecules* 14 (2013) 3997–4008, 10.1021/bm4011062. [PubMed: 24093541]
- [47]. Kikuchi T, Shimizu T, Wada M, Yamato M, Okano T, Automatic fabrication of 3-dimensional tissues using cell sheet manipulator technique, *Biomaterials* 35 (2014) 2428–2435, 10.1016/j.biomaterials.2013.12.014. [PubMed: 24370007]
- [48]. Chen AK-L, Reuveny S, Oh SKW, Application of human mesenchymal and pluripotent stem cell microcarrier cultures in cellular therapy: achievements and future direction, *Biotechnol. Adv.* 31 (2013) 1032–1046, 10.1016/j.biotechadv.2013.03.006. [PubMed: 23531528]
- [49]. Lo YMD, Tein MSC, Lau TK, Haines CJ, Leung TN, Poon PMK, Wainscoat JS, Johnson PJ, Chang AMZ, Hjelm NM, Quantitative analysis of fetal DNA in maternal plasma and



- serum: implications for noninvasive prenatal diagnosis, *Am. J. Hum. Genet.* 62 (1998) 768–775, 10.1086/301800. [PubMed: 9529358]
- [50]. He J, Mo D, Chen J, Luo L, Combined whole-mount fluorescence in situ hybridization and antibody staining in zebrafish embryos and larvae, *Nat. Protoc.* 15 (2020) 3361–3379, 10.1038/s41596-020-0376-7. [PubMed: 32908315]
- [51]. Sommer C, Straehle C, Kothe U, Hamprecht FA, Ilastik: interactive learning and segmentation toolkit, in: *Proc. - Int. Symp. Biomed. Imaging*, 2011, pp. 230–233, 10.1109/ISBI.2011.5872394.
- [52]. Chaudhuri S, Nguyen H, Rangayyan RM, Walsh S, Frank CB, A Fourier domain directional filtering method for analysis of collagen alignment in ligaments, *IEEE Trans. Biomed. Eng.* 34 (1987) 509–518, 10.1109/TBME.1987.325980. [PubMed: 3610201]
- [53]. Norris SCP, Soto J, Kasko AM, Li S, Photodegradable polyacrylamide gels for dynamic control of cell functions, *ACS Appl. Mater. Interfaces* 13 (2021) 5929–5944, 10.1021/acscami.0c19627. [PubMed: 33502154]
- [54]. Petroll MW, Cavanagh DH, Barry P, Andrews P, Jester JV, Quantitative analysis of stress fiber orientation during corneal wound contraction, *J. Cell Sci.* 104 (1993) 353–363, 10.1016/S0261-5614(03)00031-1. [PubMed: 8505365]
- [55]. Baziwane D, He Q, Gelatin: the paramount food additive, *Food Rev. Int.* 19 (2003) 423–435, 10.1081/FRI-120025483.
- [56]. Bode F, Da Silva MA, Drake AF, Ross-Murphy SB, Dreiss CA, Enzymatically cross-linked tilapia gelatin hydrogels: physical, chemical, and hybrid networks, *Biomacromolecules* 12 (2011) 3741–3752, 10.1021/bm2009894. [PubMed: 21819136]
- [57]. Kieliszek M, Misiewicz A, Microbial transglutaminase and its application in the food industry. A review, *Folia Microbiol. (Praha)* 59 (2014) 241–250, 10.1007/s12223-013-0287-x. [PubMed: 24198201]
- [58]. Darling NJ, Sideris E, Hamada N, Carmichael ST, Segura T, Injectable and spatially patterned microporous annealed particle (MAP) hydrogels for tissue repair applications, *Adv. Sci.* 5 (2018) 1–8, 10.1002/advs.201801046.
- [59]. Truong NF, Kurt E, Tahmizyan N, Leshner-Pérez SC, Chen M, Darling NJ, Xi W, Segura T, Microporous annealed particle hydrogel stiffness, void space size, and adhesion properties impact cell proliferation, cell spreading, and gene transfer, *Acta Biomater.* 94 (2019) 160–172, 10.1016/j.actbio.2019.02.054. [PubMed: 31154058]
- [60]. Bauer A, Gu L, Kwee B, Li WA, Dellacherie M, Celiz AD, Mooney DJ, Hydrogel substrate stress-relaxation regulates the spreading and proliferation of mouse myoblasts, *Acta Biomater.* 62 (2017) 82–90, 10.1016/j.actbio.2017.08.041. [PubMed: 28864249]
- [61]. Bode F, da Silva MA, Smith P, Lorenz CD, McCullen S, Stevens MM, Dreiss CA, Hybrid gelation processes in enzymatically gelled gelatin: impact on nanostructure, macroscopic properties and cellular response, *Soft Matter* 9 (2013) 6986–6999, 10.1039/C3SM00125C. [PubMed: 25310528]
- [62]. Guillou L, Babataheri A, Puech P-H, Barakat AI, Husson J, Dynamic monitoring of cell mechanical properties using profile microindentation, *Sci. Rep.* 6 (2016), 21529, 10.1038/srep21529. [PubMed: 26857265]
- [63]. Blau H, Pavlath G, Hardeman E, Chiu C, Silberstein L, Webster S, Miller S, Webster C, Plasticity of the differentiated state, *Science* 230 (1985) 758–766, 10.1126/science.2414846, 80. [PubMed: 2414846]
- [64]. Burattini S, Ferri R, Battistelli M, Curci R, Luchetti F, Falcieri E, C2C12 murine myoblasts as a model of skeletal muscle development: morpho-functional characterization, *Eur. J. Histochem.* 48 (2004) 223–233, 10.4081/891. [PubMed: 15596414]
- [65]. Rosso F, Giordano A, Barbarisi M, Barbarisi A, From Cell-ECM interactions to tissue engineering, *J. Cell. Physiol.* 199 (2004) 174–180, 10.1002/jcp.10471. [PubMed: 15039999]
- [66]. Torgan CE, Daniels MP, Regulation of myosin heavy chain expression during rat skeletal muscle development in vitro, *Mol. Biol. Cell* 12 (2001) 1499–1508, 10.1091/mbc.12.5.1499. [PubMed: 11359938]

- [67]. Ferrari C, Balandras F, Guedon E, Olmos E, Chevalot I, Marc A, Limiting cell aggregation during mesenchymal stem cell expansion on microcarriers, *Biotechnol. Prog.* 28 (2012) 780–787, 10.1002/btpr.1527. [PubMed: 22374883]
- [68]. Torgan CE, Burge SS, Collinworth AM, Truskey GA, Kraus WE, Differentiation of mammalian skeletal muscle cells cultured on microcarrier beads in a rotating cell culture system, *Med. Biol. Eng. Comput.* 38 (2000) 583–590, 10.1007/BF02345757. [PubMed: 11094818]
- [69]. Vajanthri KY, Sidu RK, Poddar S, Singh AK, Mahto SK, Combined substrate micropatterning and FFT analysis reveals myotube size control and alignment by contact guidance, *Cytoskeleton* 76 (2019) 269–285, 10.1002/cm.21527. [PubMed: 31074945]
- [70]. Ramdas NM, Qingsen Li GV, Shivashankar, Regulation of nuclear morphology by actomyosin components and cell geometry, in: 2015 37th Annu. Int. Conf. IEEE Eng. Med. Biol. Soc, IEEE, 2015, pp. 342–345, 10.1109/EMBC.2015.7318369.
- [71]. Ramdas NM, Shivashankar GV, Cytoskeletal control of nuclear morphology and chromatin organization, *J. Mol. Biol.* 427 (2015) 695–706, 10.1016/j.jmb.2014.09.008. [PubMed: 25281900]
- [72]. Bruusgaard JC, Liestøl K, Ekmark M, Kollstad K, Gundersen K, Number and spatial distribution of nuclei in the muscle fibres of normal mice studied in vivo, *J. Physiol.* 551 (2003) 467–478, 10.1113/jphysiol.2003.045328. [PubMed: 12813146]
- [73]. McClelland RE, Dennis R, Reid LM, Stegemann JP, Palsson B, Macdonald JM, Tissue engineering, in: *Introd. To Biomed. Eng.*, Elsevier, 2012, pp. 273–357, 10.1016/B978-0-12-374979-6.00006-X.
- [74]. Lim GJ, Kang S-J, Lee JY, Novel invasion indices quantify the feed-forward facilitation of tumor invasion by macrophages, *Sci. Rep.* 10 (2020) 718, 10.1038/s41598-020-57517-6. [PubMed: 31959808]
- [75]. Pereira PMR, Berisha N, Bhupathiraju NVSDK, Fernandes R, Tomé JPC, Drain CM, Cancer cell spheroids are a better screen for the photodynamic efficiency of glycosylated photosensitizers, *PLoS One* 12 (2017) 1–21, 10.1371/journal.pone.0177737.
- [76]. Dance A, Engineering the animal out of animal products, *Nat. Biotechnol.* 35 (2017) 704–707, 10.1038/nbt.3933. [PubMed: 28787425]
- [77]. Zeeb B, Saberi AH, Weiss J, McClements DJ, Formation and characterization of filled hydrogel beads based on calcium alginate: factors influencing nanoemulsion retention and release, *Food Hydrocolloids* 50 (2015) 27–36, 10.1016/j.foodhyd.2015.02.041.
- [78]. Bekhit M, Arab-Tehrany E, Kahn C, Cleymand F, Fleutot S, Desobry S, Sánchez-González L, Bioactive films containing alginate-pectin composite microbeads with *Lactococcus lactis* subsp. *lactis*: physicochemical characterization and antilisterial activity, *Int. J. Mol. Sci.* 19 (2018) 574, 10.3390/ijms19020574. [PubMed: 29443907]
- [79]. Belš ak-Cvitanovi A, Buši A, Bariši L, Vrsaljko D, Karlovi S, Špoljari I, Vojvodi A, Mrši G, Komes D, Emulsion templated microencapsulation of dandelion (*Taraxacum officinale* L.) polyphenols and  $\beta$ -carotene by ionotropic gelation of alginate and pectin, *Food Hydrocolloids* 57 (2016) 139–152, 10.1016/j.foodhyd.2016.01.020.
- [80]. Nyberg KD, Scott MB, Bruce SL, Gopinath AB, Bikos D, Mason TG, Kim JW, Choi HS, Rowat AC, The physical origins of transit time measurements for rapid, single cell mechanotyping, *Lab Chip* 16 (2016) 3330–3339, 10.1039/c6lc00169f. [PubMed: 27435631]
- [81]. Lee CH, Chin KB, Effects of pork gelatin levels on the physicochemical and textural properties of model sausages at different fat levels, *LWT* 74 (2016) 325–330, 10.1016/j.lwt.2016.07.032.
- [82]. Zhang W, Tainaka K, Ahn S, Watanabe H, Kitagawa T, Experimental and numerical investigation of effects of particle shape and size distribution on particles' dispersion in a coaxial jet flow, *Adv. Powder Technol.* 29 (2018) 2322–2330, 10.1016/j.apt.2018.06.008.
- [83]. Humbird D, Scale-up economics for cultured meat, *Biotechnol. Bioeng.* 118 (2021) 3239–3250, 10.1002/bit.27848. [PubMed: 34101164]
- [84]. Yamane A, Takahashi K, Mayo M, Vo H, Shum L, Zeichner-David M, Slavkin H, Induced expression of MyoD, myogenin and desmin during myoblast differentiation in embryonic mouse tongue development, *Arch. Oral Biol.* 43 (1998) 407–416, 10.1016/S0003-9969(98)00018-1. [PubMed: 9681116]

- [85]. Seah JSH, Singh S, Tan LP, Choudhury D, Scaffolds for the manufacture of cultured meat, *Crit. Rev. Biotechnol.* 42 (2022) 311–323, 10.1080/07388551.2021.1931803. [PubMed: 34151657]
- [86]. Kelly JY, DeSimone JM, Shape-specific, monodisperse nano-molding of protein particles, *J. Am. Chem. Soc.* 130 (2008) 5438–5439, 10.1021/ja8014428. [PubMed: 18376832]
- [87]. Wu CY, Stoecklein D, Kommajosula A, Lin J, Owsley K, Ganapathysubramanian B, Di Carlo D, Shaped 3D microcarriers for adherent cell culture and analysis, *Microsyst. Nanoeng.* 4 (2018), 10.1038/s41378-018-0020-7.
- [88]. YekrangSafakar A, Acun A, Choi J-W, Song E, Zorlutuna P, Park K, Hollow microcarriers for large-scale expansion of anchorage-dependent cells in a stirred bioreactor, *Biotechnol. Bioeng.* 115 (2018) 1717–1728, 10.1002/bit.26601. [PubMed: 29578573]
- [89]. Park W, Jang S, Kim TW, Bae J, Oh TI, Lee E, Microfluidic-printed microcarrier for in vitro expansion of adherent stem cells in 3D culture platform, *Macromol. Biosci.* 19 (2019), 1900136, 10.1002/mabi.201900136.
- [90]. Reuveny S, Silberstein L, Shahar A, Freeman E, Mizrahi A, DE-52 and DE-53 cellulose microcarriers, *In Vitro* 18 (1982) 92–98, 10.1007/BF02796400. [PubMed: 6177623]
- [91]. Li Y, Chen P, Wang Y, Yan S, Feng X, Du W, Koehler SA, Demirci U, Liu BF, Rapid assembly of heterogeneous 3D cell microenvironments in a microgel array, *Adv. Mater.* 28 (2016) 3543–3548, 10.1002/adma.201600247. [PubMed: 26991071]
- [92]. Jeon SJ, Hayward RC, Reconfigurable microscale frameworks from concatenated helices with controlled chirality, *Adv. Mater.* 29 (2017) 1–7, 10.1002/adma.201606111.
- [93]. Hu Y, Wang Q, Wang J, Zhu J, Wang H, Yang Y, Shape controllable microgel particles prepared by microfluidic combining external ionic crosslinking, *Biomicrofluidics* 6 (2012) 1–9, 10.1063/1.4720396.
- [94]. Li M, Joung D, Hughes B, Waldman SD, Kozinski JA, Hwang DK, Wrinkling non-spherical particles and its application in cell attachment promotion, *Sci. Rep.* 6 (2016) 1–9, 10.1038/srep30463. [PubMed: 28442746]
- [95]. Wang P-Y, Li W-T, Yu J, Tsai W-B, Modulation of osteogenic, adipogenic and myogenic differentiation of mesenchymal stem cells by submicron grooved topography, *J. Mater. Sci. Mater. Med.* 23 (2012) 3015–3028, 10.1007/s10856-012-4748-6. [PubMed: 22903603]
- [96]. Jin W, Tamzalit F, Chaudhuri PK, Black CT, Huse M, Kam LC, T cell activation and immune synapse organization respond to the microscale mechanics of structured surfaces, *Proc. Natl. Acad. Sci.* 116 (2019), 19835, 10.1073/pnas.1906986116. –19840. [PubMed: 31527238]
- [97]. Park S, Kim D, Park S, Kim S, Lee D, Kim W, Kim J, Nanopatterned Scaffolds for Neural Tissue Engineering and Regenerative Medicine, 2018, pp. 421–443, 10.1007/978-981-13-0950-2\_22.
- [98]. Campiglio CE, Negrini NC, Farè S, Draghi L, Cross-linking strategies for electrospun gelatin scaffolds, *Materials (Basel)* 12 (2019), 10.3390/ma12152476.
- [99]. Leal-Calderon F, Thivilliers F, Schmitt V, Structured emulsions, *Curr. Opin. Colloid Interface Sci.* 12 (2007) 206–212, 10.1016/j.cocis.2007.07.003.
- [100]. Saito M, Yin L, Kobayashi I, Nakajima M, Preparation characteristics of monodispersed oil-in-water emulsions with large particles stabilized by proteins in straight-through microchannel emulsification, *Food Hydrocolloids* 19 (2005) 745–751, 10.1016/j.foodhyd.2004.08.005.
- [101]. Neufeld RJ, Poncelet D, Industrial Scale Encapsulation of Cells Using Emulsification/Dispersion Technologies, 2004, pp. 311–325, 10.1007/978-94-017-1638-3\_17.
- [102]. Poncelet D, Lencki R, Beaulieu C, Halle JP, Neufeld RJ, Fournier A, Production of alginate beads by emulsification/internal gelation. I. Methodology, *Appl. Microbiol. Biotechnol.* 38 (1992) 39–45, 10.1007/BF00169416. [PubMed: 1369009]
- [103]. McMurtrey RJ, Analytic models of oxygen and nutrient diffusion, metabolism dynamics, and architecture optimization in three-dimensional tissue constructs with applications and insights in cerebral organoids, *Tissue Eng. Part C Methods* 22 (2016) 221–249, 10.1089/ten.tec.2015.0375. [PubMed: 26650970]
- [104]. Chen H-C, Hu Y-C, Bioreactors for tissue engineering, *Biotechnol. Lett.* 28 (2006) 1415–1423, 10.1007/s10529-006-9111-x. [PubMed: 16955350]

- [105]. Horiike M, Ogawa Y, Kawada S, Effects of hyperoxia and hypoxia on the proliferation of C2C12 myoblasts, *Am. J. Physiol. Integr. Comp. Physiol.* 321 (2021) R572, 10.1152/ajpregu.00269.2020. –R587.
- [106]. Chakravarthy MV, Spangenburg EE, Booth FW, Culture in low levels of oxygen enhances in vitro proliferation potential of satellite cells from old skeletal muscles, *Cell. Mol. Life Sci.* 58 (2001) 1150–1158, 10.1007/PL00000929. [PubMed: 11529507]
- [107]. Totland GK, Kryvi H, Slinde E, Composition of muscle fibre types and connective tissue in bovine *M. semitendinosus* and its relation to tenderness, *Meat Sci.* 23 (1988) 303–315, 10.1016/0309-1740(88)90014-9. [PubMed: 22055745]
- [108]. Weston AR, Rogers RW, Althen TG, Review: the role of collagen in meat tenderness, *Prof. Anim. Sci.* 18 (2002) 107–111, 10.15232/S1080-7446(15)31497-2.
- [109]. Cheng CS, Parrish FC, Scanning electron microscopy of bovine muscle: effect of heating on ultrastructure, *J. Food Sci.* 41 (1976) 1449–1454, 10.1111/j.1365-2621.1976.tb01193.x.
- [110]. Stephens N, Ruivenkamp M, Promise and ontological ambiguity in the in vitro meat imagescape: from laboratory myotubes to the cultured burger, *Sci. Cult. (Lond)* 25 (2016) 327–355, 10.1080/09505431.2016.1171836. [PubMed: 27695202]
- [111]. Schaafsma G, The protein digestibility–corrected amino acid score, *J. Nutr.* 130 (2000) 1865S–1867S, 10.1093/jn/130.7.1865S. [PubMed: 10867064]
- [112]. Hornstein I, Crowe PF, Meat flavor chemistry, flavor studies on beef and pork, *J. Agric. Food Chem.* 8 (1960) 494–498, 10.1021/jf60112a022.

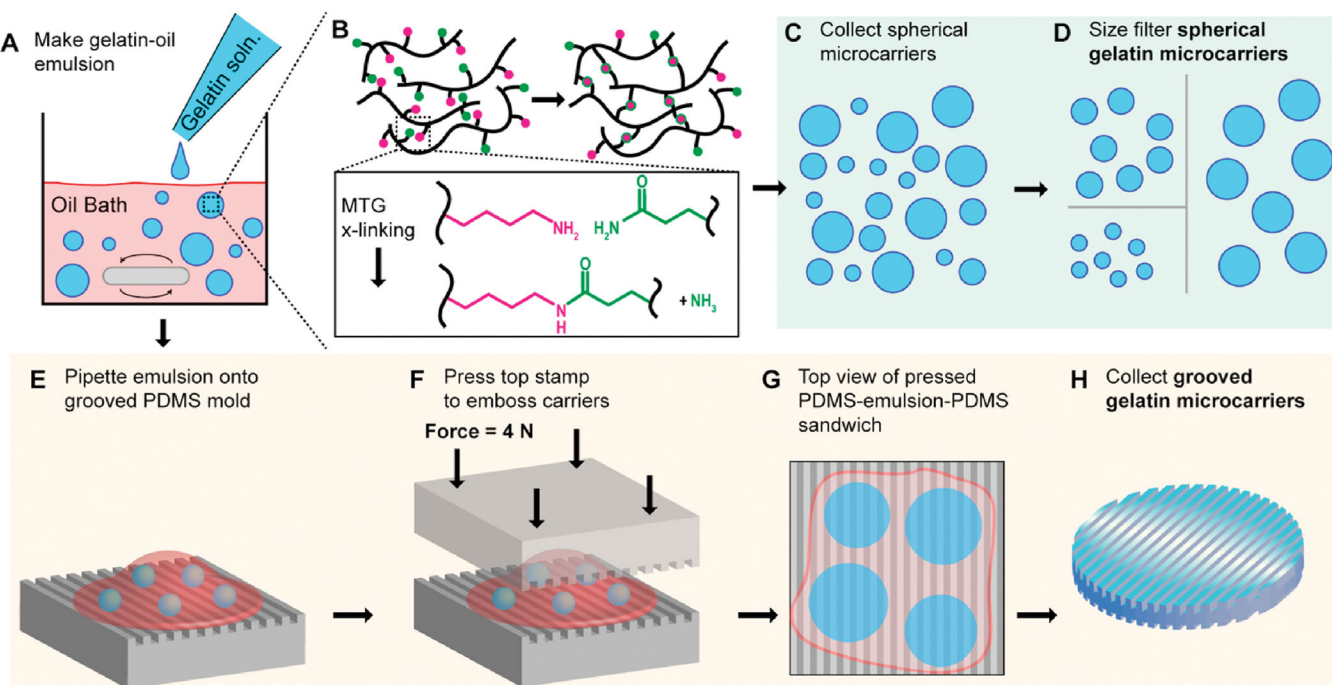


**Fig. 1.** Fabrication strategies for edible microcarriers. (A) An emulsion was formed by adding gelatin and MTG to a mineral oil bath with 1% Span 80. (B) Chemical crosslinking of gelatin occurred through an enzymatic reaction that binds glutamine and lysine side chains. (C) After breaking the emulsion, spherical microcarriers (sMCs) were suspended in PBS, and (D) the microcarriers were size filtered before use. To make grooved microcarriers (gMCs), (E) the emulsion was placed onto a grooved PDMS stamp after partial crosslinking and (F, G) confined between two PDMS stamps during crosslinking. (H) The microcarriers with grooved topology were released from the stamps and excess oil was removed before resuspending in PBS.

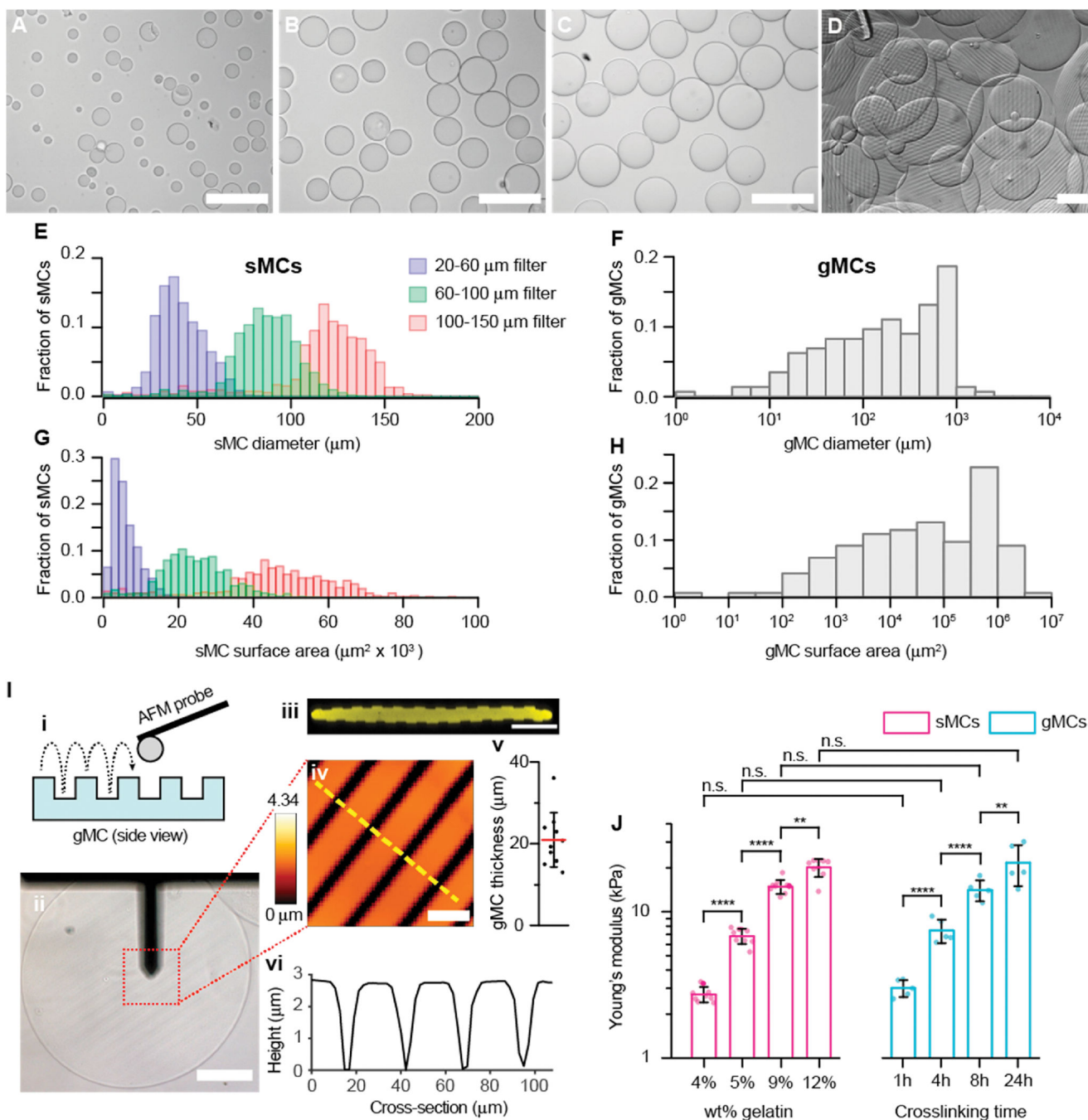


**Fig. 2.** Characterization of edible microcarriers. Phase contrast images of (A-C) spherical microcarriers (sMCs) with 9 wt% gelatin polymerized for 24 h after collecting between filters with pore sizes of (A) 20–60  $\mu\text{m}$ , (B) 60–100  $\mu\text{m}$ , and (C) 100–150  $\mu\text{m}$ . Scale, 200  $\mu\text{m}$ . (D) Grooved microcarriers (gMCs) with 9 wt% gelatin crosslinked for 8 h. Scale, 200  $\mu\text{m}$ . Example histograms showing the (E, F) diameter and (G, H) surface area per particle of collected sMCs and gMCs. sMCs are collected between filters of different pore sizes, and gMCs are collected on top of a 100  $\mu\text{m}$  filter to remove smaller objects. Histograms

represent the microcarrier diameter and surface area distributions of an entire 10  $\mu$ L aliquot. **(I)** Atomic force microscopy (AFM) and cross-sectional confocal microscopy of gMCs: **(i)** schematic of AFM probe scanning gMC surface; **(ii)** phase contrast image of AFM set up. Scale, 100  $\mu$ m; **(iii)** confocal image showing cross-section of a gMC. Scale. 50  $\mu$ m; **(iv)** AFM topology map of gMC surface. Scale, 25  $\mu$ m; **(v)** measured gMC thickness from confocal images, as shown in **(iii)** (n = 9 individual gMCs, horizontal line denotes mean  $\pm$  SD); **(vi)** example plot of microcarrier surface topology measured using AFM, which corresponds to the dashed line shown in **(iv)**. **(J)** Young's modulus of the sMCs with increasing wt% gelatin and gMCs with increasing crosslinking time (mean  $\pm$  SD). Statistical significance determined using 1-way ANOVA. (n.s. not significantly different, \*p < 0.05, \*\* < 0.01, \*\*\* < 0.001, \*\*\*\* < 0.0001; gMCs n = 5; sMCs n = 9 individual microcarriers).

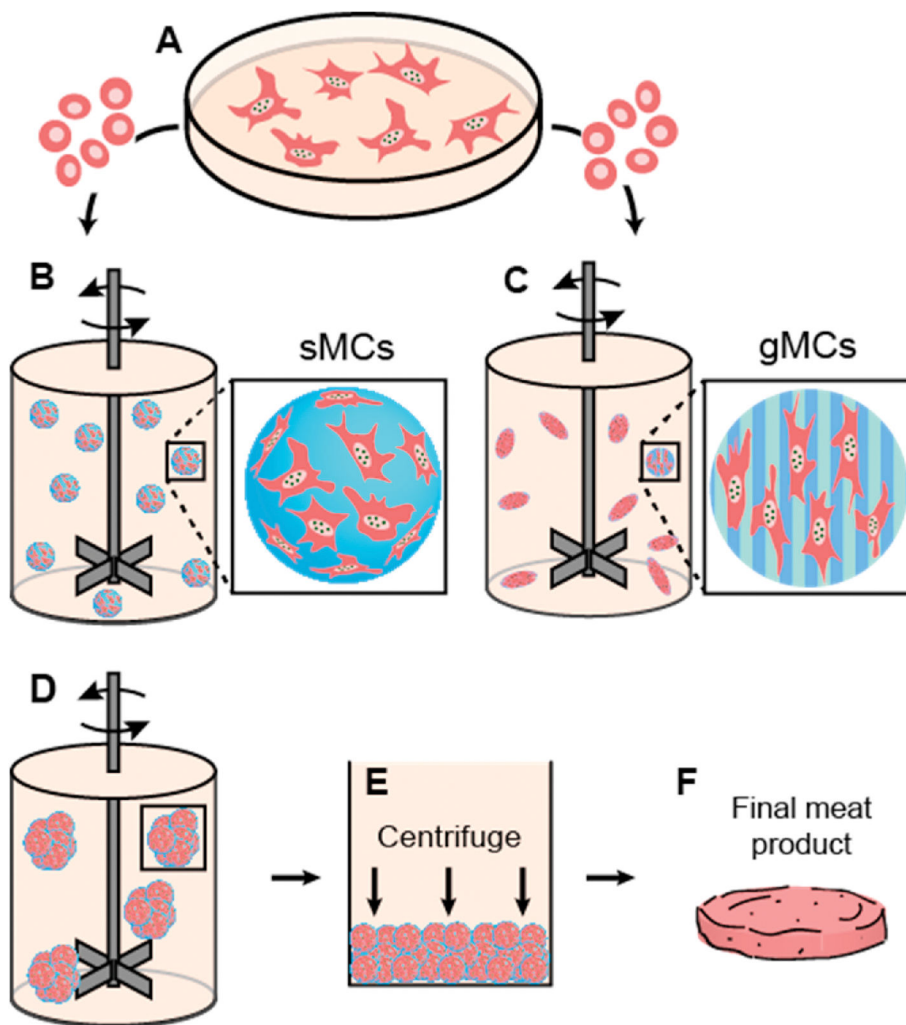


**Fig. 3.** Schematic of process flow from cells and edible microcarriers to cultured meat. **(A-C)** Cells were seeded onto edible microcarriers with tunable mechanics and surface topology. **(D)** Edible microcarriers supported myoblast expansion and differentiation and formation of cell-microcarrier structures or “microtissues.” **(E)** The microtissues were harvested by centrifugation to form **(F)** a cookable cultured meat product.



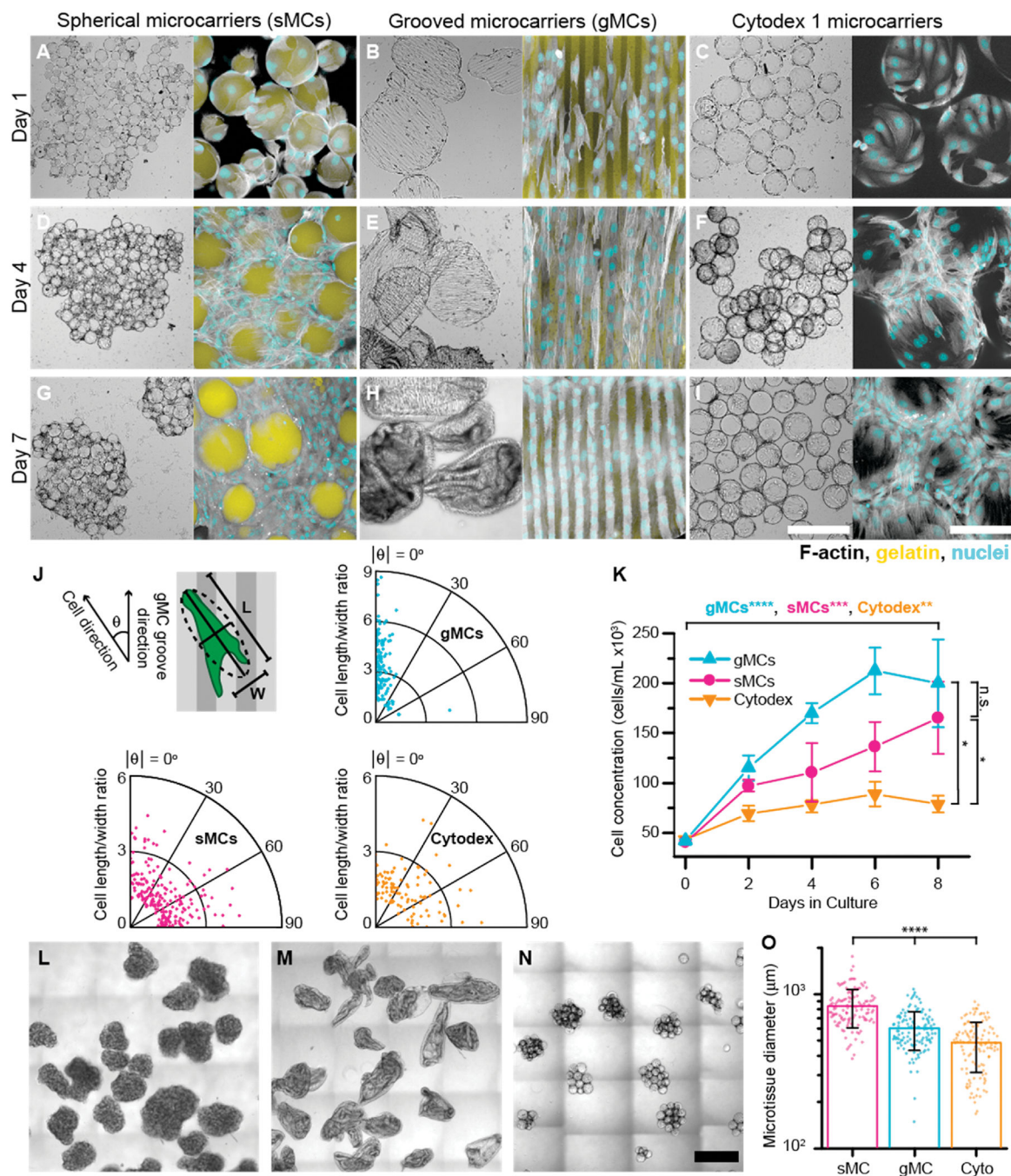


**Fig. 4.** Edible microcarriers support cell expansion. C2C12 cells were cultured on (A-C) spherical microcarriers (sMCs), (D-F) grooved microcarriers (gMCs), or (G-I) Cytodex microcarriers. Widefield (left) and confocal (right) images were acquired at (A, D, G) 1 day, (B, E, H) 4 days, and (C, F, I) 7 days after cell seeding. (J) To quantify alignment, cells on gMCs were segmented and an ellipse was fitted to the cell body. The orientation angle ( $\theta$ ) between the major axis of the fitted ellipse and gMC groove direction was plotted against the length/width ratio for each cell in polar coordinates. For cells on sMCs and Cytodex

microcarriers,  $\theta$  was determined relative to the mean cell major axis direction in the imaging window;  $n > 100$  cells on 6 separate microcarrier clusters, 2 independent experiments. **(K)** The cell concentration in the bioreactor (cells/mL of culture volume) was measured by quantifying DNA over the course of 8 days, where 1 mL cell suspension contained 8.8  $\text{cm}^2/\text{mL}$  microcarrier surface area. We report here cell concentrations assuming 6.6 pg DNA/cell (mean  $\pm$  SD) averaged over three independent experiments. Live microtissue aggregates observed for **(L)** sMCs, **(M)** gMCs, and **(N)** Cytodex microcarriers. **(O)** Distribution of microtissue aggregate diameters for each microcarrier type;  $n = 118$  aggregates, 2 independent experiments. Statistical significance determined using 1-way ANOVA. n.s. not significantly different, \* $p < 0.05$ , \*\*  $< 0.01$ , \*\*\*  $< 0.001$ , \*\*\*\*  $< 0.0001$ . Scale, **(A-I)** widefield: 500  $\mu\text{m}$ , confocal: 200  $\mu\text{m}$ , **(L-N)** 1000  $\mu\text{m}$ .

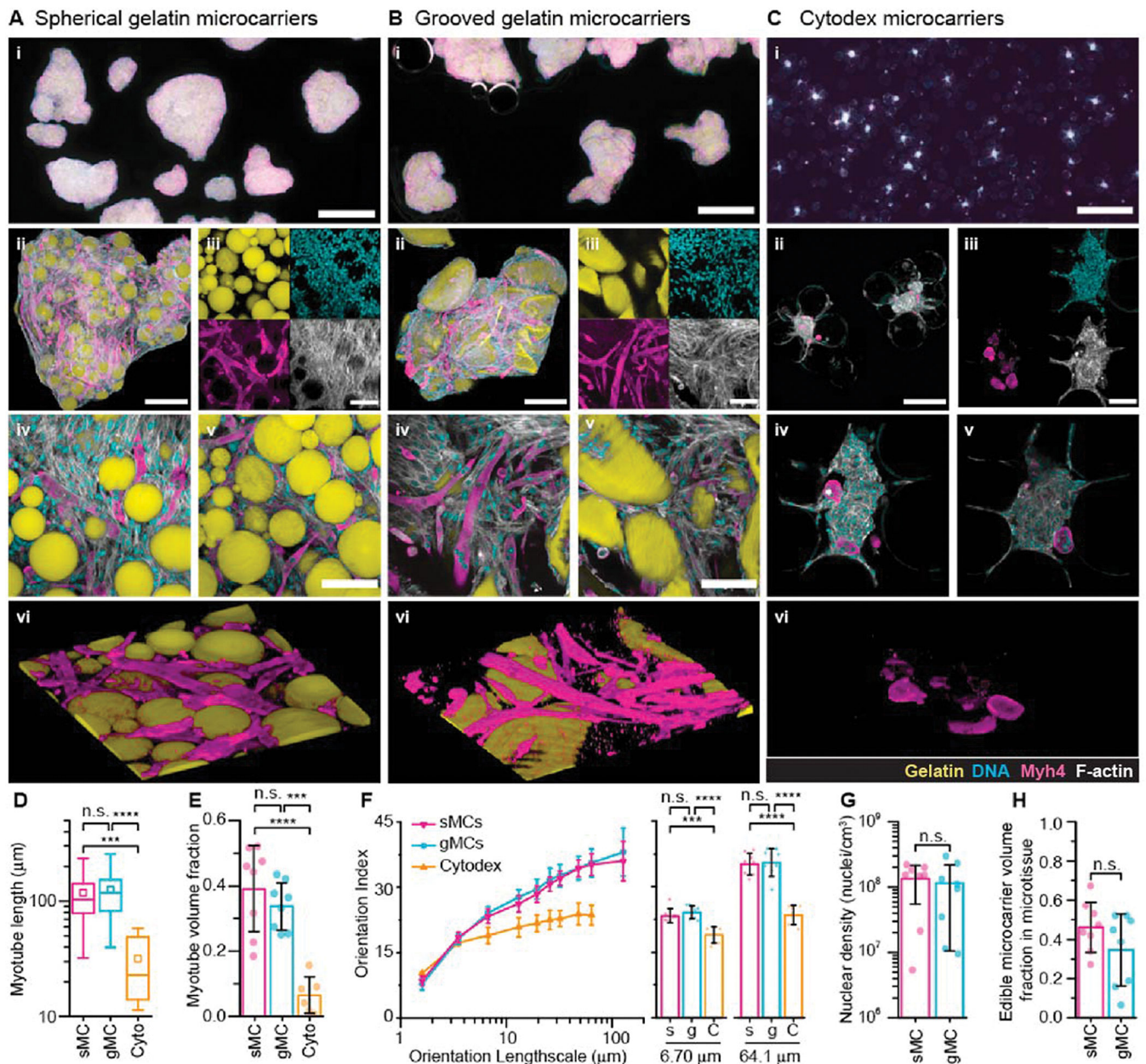


**Fig. 5.** Edible microcarriers support myotube formation. C2C12 cells were expanded and differentiated on (A) spherical microcarriers (sMCs), (B) grooved microcarriers (gMCs), and (C) Cytodex 1 microcarriers. Images show gelatin (FITC, yellow), DNA (Hoechst, cyan), myosin heavy chain (Myh4, magenta), and F-actin (phalloidin, gray). (i) Widefield images of the labeled microtissues. Scale, 1000  $\mu\text{m}$ . (ii-vi) Z-stacks were acquired with a confocal microscope. (ii) Projection of the 3D images reconstructed from the confocal slices. Scale, 200  $\mu\text{m}$ . (iii-vi) Higher magnification images. Scale, 100  $\mu\text{m}$ . (iii) Montages of maximum intensity projections of the z-stacks. Single z-slice images of regions on the (iv) outside surface and (v) interior of the microtissues. (vi) 3D-rendered images of showing myotubes and microcarriers only. (D) Length of myotubes within the imaging window. (E) Fraction of

the cellular volume that is comprised of myotubes, where cellular volume is the microtissue volume excluding microcarriers. **(F)** The orientation index of F-actin across different length scales; higher values indicate increased F-actin alignment. Bar graphs show comparisons of the orientation index at 6.70 and 64.1  $\mu\text{m}$ . Values represent the mean orientation index across confocal stacks and error bars represent standard deviation. **(G)** Densities of nuclei within the microtissues formed from sMCs and gMCS. **(H)** Microcarrier volume fraction within the microtissues.  $n = 6$  microtissues per condition across 2 independent experiments, mean  $\pm$  SD. Statistical significance determined using 1-way ANOVA. n.s. not significantly different, \* $p < 0.05$ , \*\*  $<0.01$ , \*\*\*  $<0.001$ , \*\*\*\*  $<0.0001$ .

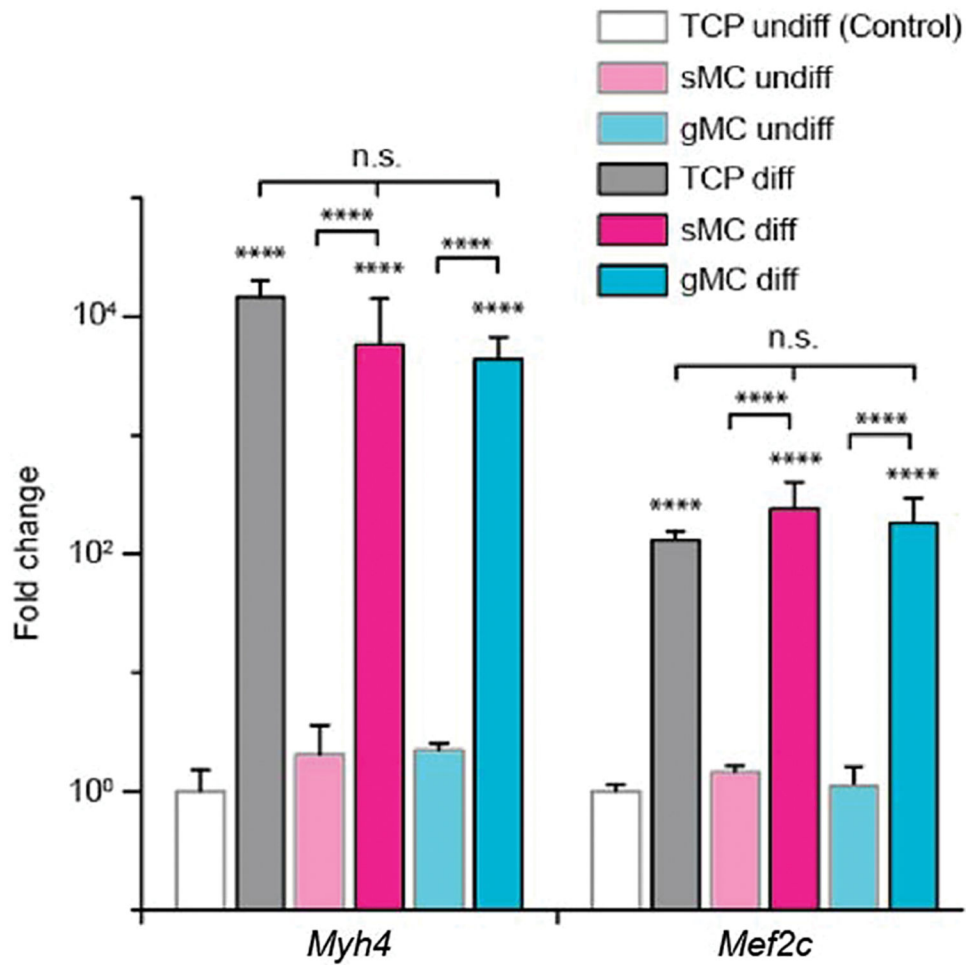


**Fig. 6.**

Levels of *Myh4* and *Mef2c* transcripts of C2C12 cells grown on tissue culture plastic (TCP), spherical microcarriers (sMCs), and grooved microcarriers (gMCs), as measured by RT-qPCR using the delta delta cycle time method ( $\Delta\Delta Ct$ ) with *Gapdh* as an endogenous control. Differentiated samples (diff) were grown for 7 days in growth media, followed by 7 days in differentiation media. Data is normalized to a control (Ctrl) of undifferentiated (undiff) C2C12 cells on tissue culture plastic (TCP) after 1 day in culture.  $n = 3$  independent experiments per condition, mean  $\pm$  SD. Statistical significance determined using one-way ANOVA. n.s. not significantly different, \*\*\*\*  $<0.0001$ . Asterisks show statistical significance of transcript levels normalized to the control.

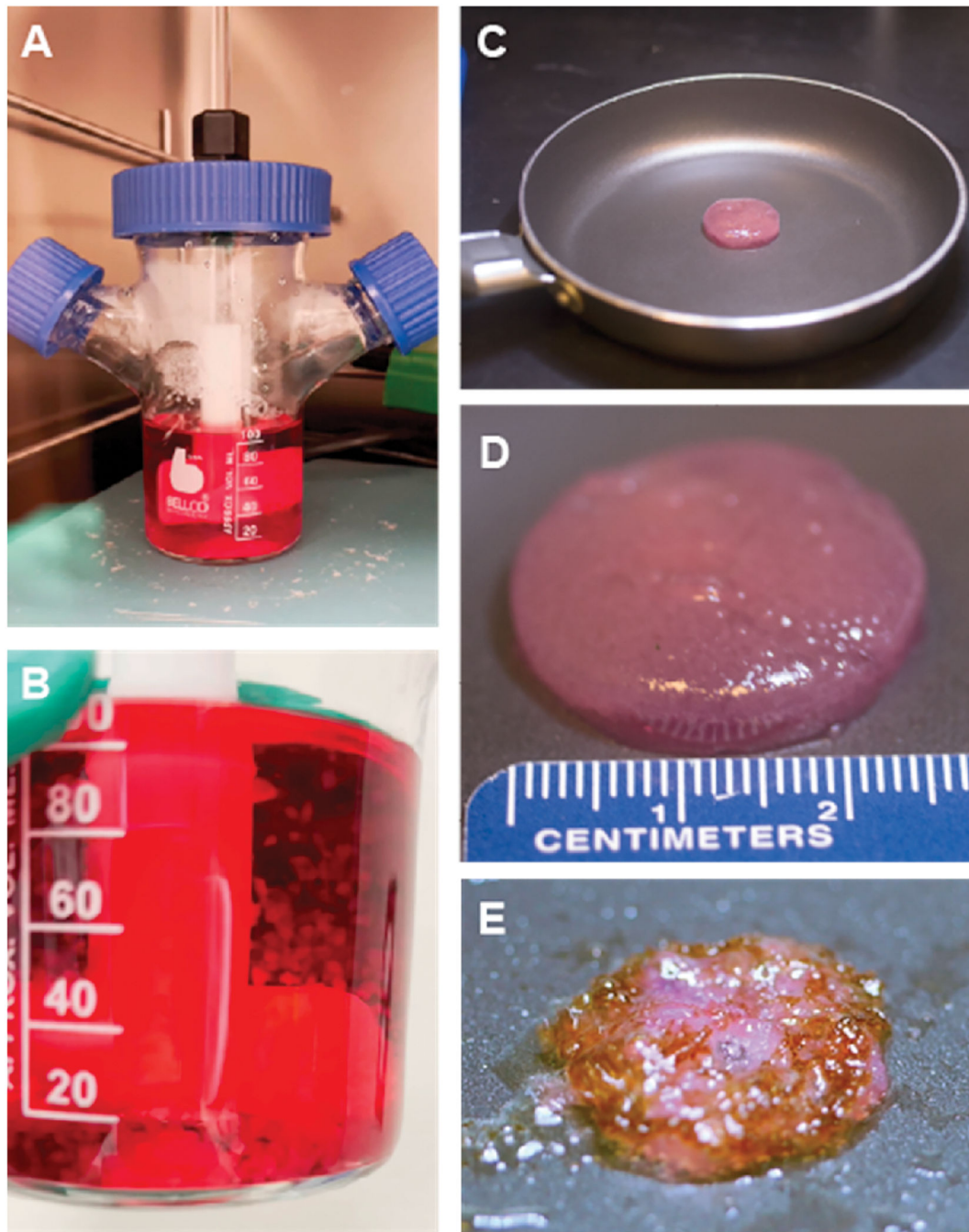


**Fig. 7.** Harvesting and cooking cultured bovine meat. Bovine satellite muscle cells (BSMCs) were cultured with sMCs. (A) Cells were expanded in a 100 mL spinner flask for 7 days before inducing differentiation for another 7 days and (B) self-assembled into microtissues during culture. (C, D) The resultant microtissues were harvested by centrifugation, formed into a cohesive meat product, and (E) cooked on a hot 195 °C griddle in olive oil after 8 min 45 s.

Composition of spherical microcarriers (sMCs) and grooved microcarriers (gMCs), stir rates at which the emulsions were mixed, crosslinking time, and resultant microcarrier stiffness (Young's modulus). Young's modulus was determined using AFM,  $n = 9$  separate microcarriers for sMCs, and  $n = 5$  for gMCs; error represents the standard deviation.

**Table 1**

Microcarrier Designation	Gelatin (mg)	Water ( $\mu$ L)	20% MTG stock ( $\mu$ L)	Stir speed (RPM)	Time of crosslinking (h)	Young's modulus (kPa)
3% sMCs	30	770	200	250	24	$0.495 \pm 0.054$
4% sMCs	40	760	200	250	24	$2.73 \pm 0.33$
5% sMCs	50	750	200	250	24	$6.84 \pm 0.82$
6% sMCs	60	740	200	300	24	$9.26 \pm 0.42$
9% sMCs	90	710	200	350	24	$14.9 \pm 1.6$
12% sMCs	120	680	200	400	24	$20.1 \pm 2.8$
1 h gMCs	90	835	75	270	1	$3.01 \pm 0.40$
4 h gMCs	90	835	75	270	4	$7.47 \pm 1.37$
8 h gMCs	90	835	75	270	8	$14.1 \pm 2.3$
24 h gMCs	90	835	75	270	24	$21.8 \pm 6.8$

**Table 2**

Primers used for RT-qPCR methods.

Primer name	Sequence
<i>Gapdh</i>	forward 5'-TGAACGGATTGGCCGTATT-3'
<i>Gapdh</i>	reverse 5'-CTGGAACATGTAGACCATGTAGTT-3'
<i>Myh4</i>	forward 5'-TCTACACTTACTCAGGCCTCTT-3'
<i>Myh4</i>	reverse 5'-CTGGTAGGCGTTATCAGAGATG-3'
<i>Mef2C</i>	forward 5'-CTGGCAGCTCTACACCATTG -3'
<i>Mef2C</i>	reverse 5'-AAGCCTTCTTCATCAATCCAAA -3'

Author Manuscript

Author Manuscript

Author Manuscript

Author Manuscript